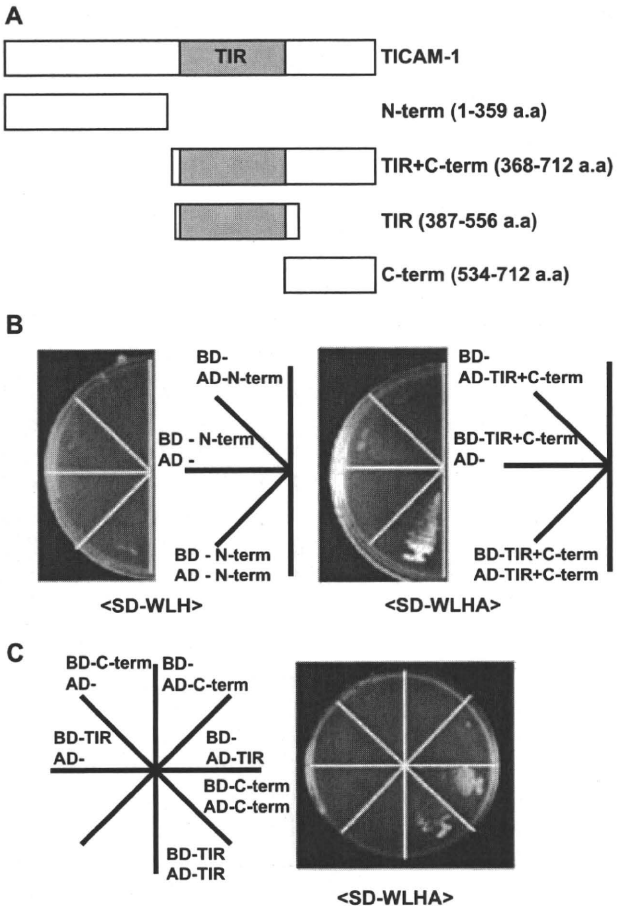

FIGURE 1. **The homodimerization motifs of TICAM-1 are located in both the TIR domain and C-terminal region.** *A*, construction of TICAM-1 mutants for the yeast two-hybrid assay. Each truncated TICAM-1 construct, N-term (1–359 aa), TIR+C-term (368–712 aa), TIR (387–556 aa), or C-term (534–712 aa), was inserted into the pGBKT7 (bait) and the pGADT7 (prey) vectors. The *shaded box* represents the TIR domain of TICAM-1 (394–533 aa). *B* and *C*, homodimerization of the TICAM-1 mutants in yeast. The TICAM-1 mutant containing the N-terminal region (*N-term*) failed to homodimerize (*B*, *left panel*), whereas the TICAM-1 mutant containing the TIR domain and C-terminal region (*TIR+C-term*) was homodimerized in yeast (*B*, *right panel*). The TICAM-1 mutants containing only the TIR domain or C-terminal region were homodimerized in the WLHA plate (*C*). *BD* and *AD* represent the bait and prey plasmids, respectively. *SD-WLH* reflects a weak interaction; *SD-WLHA* reflects a strong interaction.

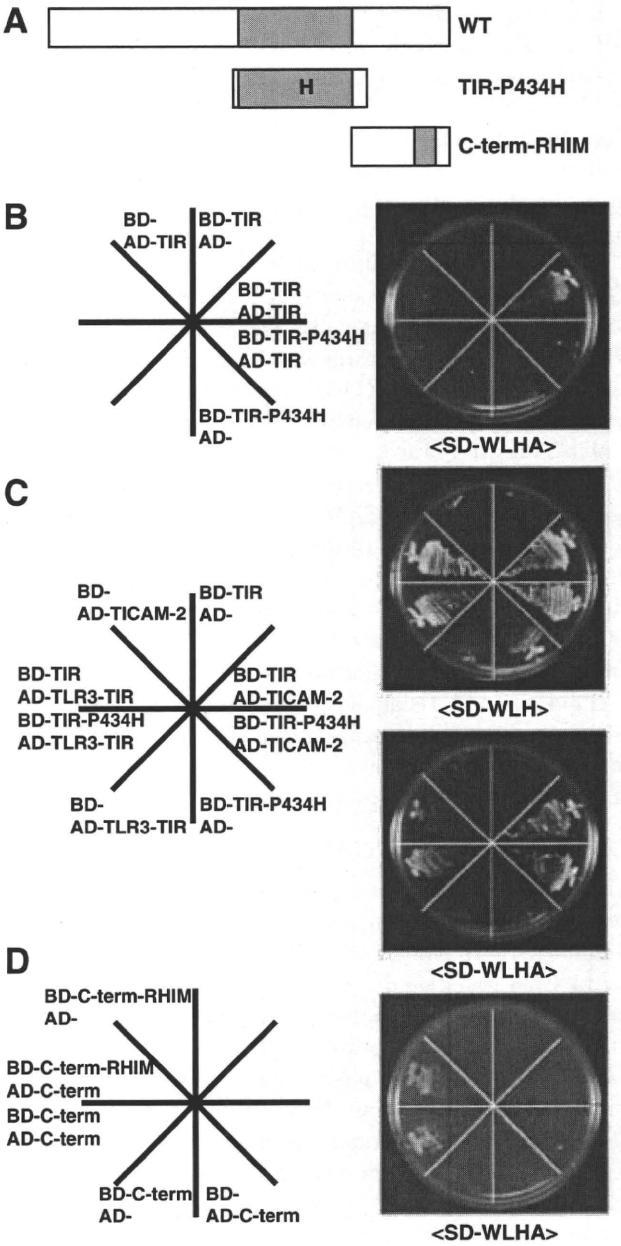

FIGURE 2. **Proline 434 in the TIR domain is critical for homodimerization of TICAM-1 but not for association with TLR3 or TICAM-2.** *A*, construction of TICAM-1 mutants for the yeast two-hybrid assay. The constructs of the TICAM-1 mutant, TIR-P434H (387–556 aa, Pro^{434} in the TIR domain is replaced by His) and C-term-RHIM (534–712 aa, ^{587}VQLG^{690} within the RHIM domain are replaced with four Ala) were inserted into the pGBKT7 (bait) and the pGADT7 (prey) vectors. *B* and *C*, interactions between the TICAM-1mutant (TIR-P434H) and wild-type TICAM-1-TIR (TIR), TLR3-TIR, or TICAM-2 in the yeast two-hybrid system. No association was detected between the mutated TIR (TIR-P434H) and wild-type TICAM-1-TIR (*B*), whereas strong association was observed between the TIR-P434H mutant and the TIR of TLR3 (755–904 aa) or TICAM-2 (*C*). *D*, interaction between the C-terminal of TICAM-1 with its RHIM mutant. Association between the RHIM mutant and wild-type C-terminal of TICAM-1 was observed. *BD* and *AD* represent the bait and prey plasmids, respectively.

taining 150 mM NaCl, 1% Nonidet P-40, 10 mM EDTA, 25 mM iodoacetamide, 2 mM phenylmethylsulfonyl fluoride, and a protease inhibitor mixture (Roche Applied Science)). Lysates were clarified by centrifugation, pre-cleared with Protein G-Sepharose (GE Healthcare, Buckinghamshire, UK), and incubated with 0.5–2.5 μg of Abs. The immunocomplexes were recovered by incubation with Protein G-Sepharose, washed three times with lysis buffer, and resuspended in denaturing buffer. Samples were analyzed by SDS-PAGE (7.5–10%) under reducing conditions followed by immunoblotting with anti-tag Abs.

RESULTS

TICAM-1 Homodimerizes via the TIR Domain and C-terminal Region in Yeast—Upon dsRNA stimulation, TICAM-1 transiently associates with TLR3 before forming a speckle-like structure with downstream signaling molecules (25). The topological dynamics of TICAM-1 secondary to activation by dsRNA-TLR3 remains unknown, although currently accepted view is that the interaction between TLR3-TIR and TICAM-1-TIR is important for clustering the adaptor molecules around the receptor. Furthermore, overexpressed TICAM-1 forms speckle-like signalosomes in a TLR3-independent manner (25). To examine TICAM-1 oligomerization, we generated several

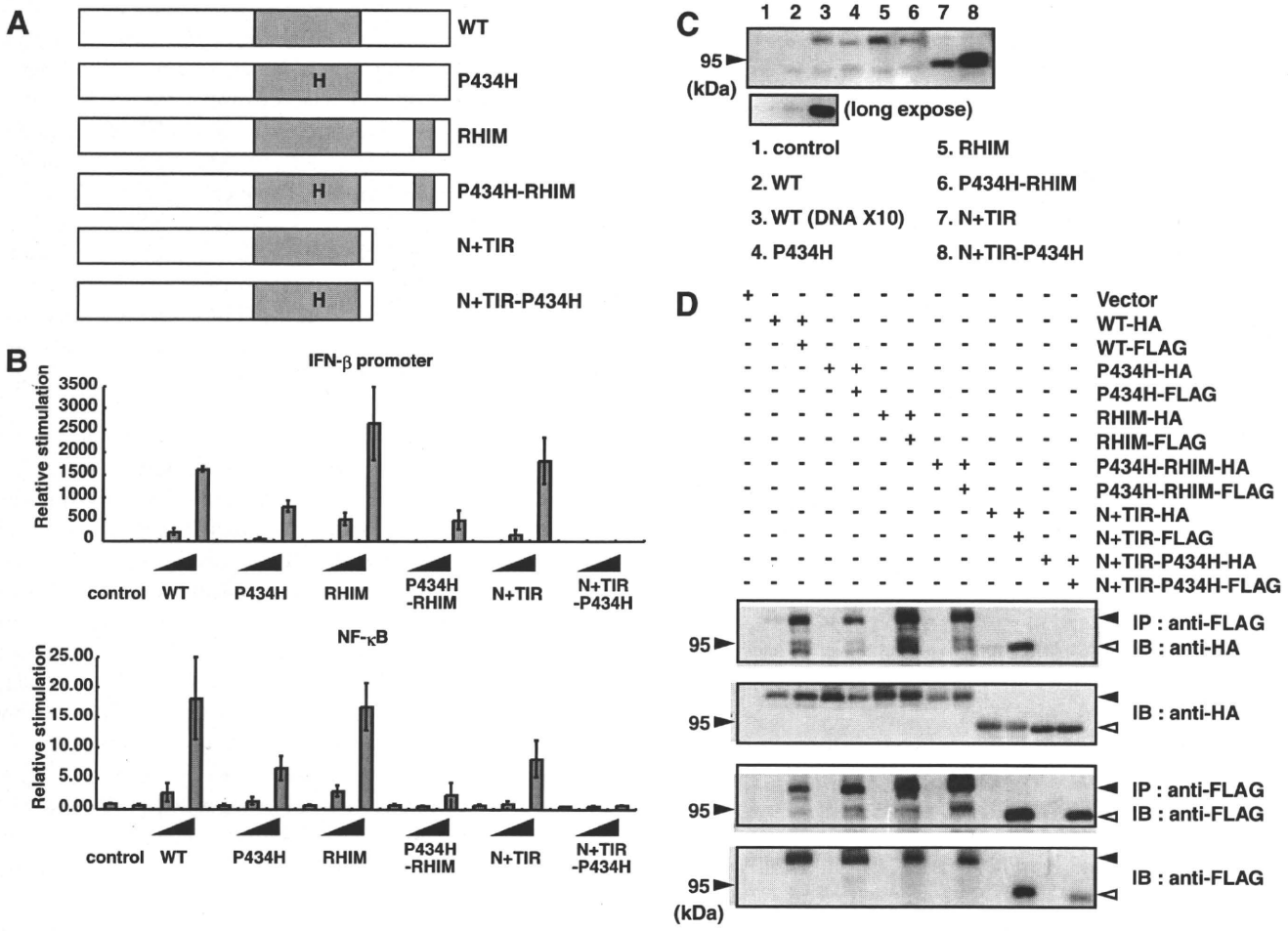

FIGURE 3. **Pro^{434} in the TIR domain and the C-terminal RHIM domain are required for full activation of TICAM-1.** *A*, constructs of various TICAM-1 mutants were used. The mutant P434H construct contains a mutated TIR domain in which Pro^{434} is substituted with His. The mutant RHIM construct contains a mutated RHIM domain (^{587}VQLG^{690} are replaced with four Ala). The mutant P434H-RHIM construct has two mutated sites, Pro^{434} and RHIM. The mutant N+TIR (1–566 aa) contains the N-terminal region and the TIR domain and the mutant N+(TIR-P434H) contains the N-terminal region with the mutated TIR-P434H domain. *B*, Pro^{434} in the TIR domain and the RHIM domain play an important role in TICAM-1-mediated NF-κB and IFN-β promoter activation. HEK293 cells in 96-well plates were transfected with the indicated expression plasmids (0.2, 2.0, and 20.0 ng) together with the IFN-β promoter reporter (*upper panel*, 100 ng) or NF-κB reporter plasmids (*lower panel*, 100 ng), and phRL-TK (1.0 ng). Twenty-four hours after transfection, the luciferase reporter activities were measured. The average activities from three independent assays are shown as relative stimulation. *C*, HEK293 cells in 24-well plates were transfected with expression plasmids for HA-tagged wild-type TICAM-1 (20 and 200 ng) or each TICAM-1 mutant (20 ng) in the presence of an apoptosis inhibitor. Protein expression levels were determined by immunoblotting using anti-HA pAb. The protein levels of the TICAM-1 mutants are significantly higher than that of wild-type TICAM-1 using the same concentration of DNA plasmid. *Lower panel*, long exposed membrane. *D*, the homodimerizing ability of the TICAM-1 mutants was assessed using a co-immunoprecipitation assay. HEK293 cells were transfected with the indicated plasmids for HA- or FLAG-tagged TICAM-1 mutants, and cell lysates were immunoprecipitated with anti-FLAG mAb. Immunoprecipitants were resolved on SDS-PAGE under reducing conditions followed by immunoblotting with anti-HA pAb or anti-FLAG mAb. The protein expression in the total cell lysates was analyzed by immunoblotting with anti-HA pAb or anti-FLAG mAb (*IB*). Only the N+(TIR-P434H) mutant did not homodimerized (*upper panel*). *Closed arrowheads* indicate full-length TICAM-1, and *open arrowheads* indicate the truncated form of TICAM-1 (N+TIR).

truncated TICAM-1 constructs and assayed their homodimerization activities using the yeast two-hybrid system (Fig. 1*A*). The construct containing the TIR domain and C-terminal region of TICAM-1 induced homodimerization, whereas the construct containing the N-terminal region alone did not (Fig. 1*B*). Of the constructs that had been truncated further, only the TIR domain or C-terminal region was homodimerized in the yeast system (Fig. 1*C*) suggesting that TICAM-1 oligomerization is mediated through the TIR domain and C-terminal region.

TICAM-1 Dimerization Requires the Pro^{434} Residue in the TIR Domain and the C-terminal Region with the Exception of the RHIM Domain—We have previously reported that the TIR domain TIR-P434H mutant acts as a dominant-negative form during TLR3-mediated signaling (7). In the yeast two-hybrid system, TIR-P434H failed to interact with the TIR domain of TICAM-1 but bound tightly to the tail of TLR3 or TICAM-2 (Figs. 2, *A–C*). These findings suggest that Pro^{434} is critical for the TICAM-1 signaling that mediates TICAM-1 dimerization via the TIR domain. To further identify residues required for mediating TICAM-1 dimerization through the C-terminal region, we generated a TICAM-1 construct consisting of the C-terminal region with a mutated-RHIM domain (Fig. 2*A*). The RHIM domain is essential for TICAM-1-mediated NF-κB activation and induction of apoptosis via binding of RIP1 (14, 15). Mutation of the RHIM motif did not affect the dimerization of the C-terminal region (Fig. 2*D*) suggesting that the RHIM motif is dispensable for TICAM-1 dimerization via the C-terminal region.

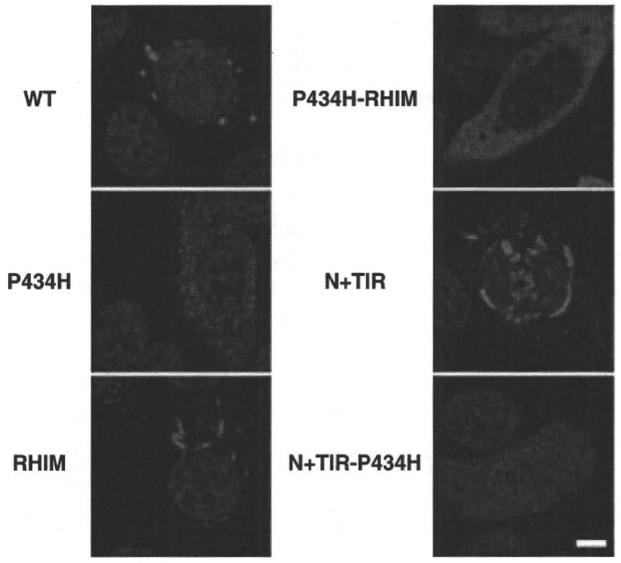

FIGURE 4. **Subcellular localization of TICAM-1 mutants.** HeLa cells were transfected with the indicated plasmids for FLAG-tagged wild-type TICAM-1 and TICAM-1 mutants and stained with anti-FLAG mAb followed by Alexa568-labeled goat anti-mouse Ab (*red*). Mutation of Pro^{434} in the TIR domain or mutation of the C-terminal RHIM domain affects the subcellular localization of TICAM-1. Nuclei were stained with DAPI (*blue*). *Bar*, 10 μm.

TICAM-1-mediated IRF-3 and NF-κB Activation Is Reduced by Mutations in the TIR or RHIM Domain—Based on the results of the yeast-two hybrid assay, we constructed several TICAM-1 mutants and examined their activities in mammalian cells (Fig. 3*A*). Only the TICAM-1 N+(TIR-P434H) mutant failed to activate both the IFN-β promoter and NF-κB, even after transfection of high concentrations of plasmid (Fig. 3*B*). The other mutants retained their IFN-β promoter and NF-κB activating abilities. However, transfection of the same concentration of plasmid resulted in increased protein expression of all TICAM-1 mutants compared with wild-type TICAM-1 protein expression (Fig. 3*C*). Subsequent normalization of the protein expression levels revealed that the signaling activities of these mutants were very weak compared with wild-type TICAM-1.

To examine the relationship between the reduced NF-κB and IFN-β promoter activation of each mutant and their homodimerizing activity, immunoprecipitation studies using HA- and FLAG-tagged constructs were performed. The homodimerizing activity was completely diminished in the dysfunctional N+(TIR-P434H) mutant (Fig. 3*D*). As observed in the yeast system, either the TIR domain or the C-terminal region enabled the TICAM-1 mutants to homodimerize in HEK293 cells. However, lack of either domain reduced the signaling activities of these mutants. These results suggest that full activation of TICAM-1 requires homodimerization at both the TIR domain and the C-terminal region.

Mutations of TICAM-1 Affect Its Subcellular Localization—To clarify the functional differences between wild-type TICAM-1 and the TICAM-1 mutants, we examined the subcellular localization of each FLAG-tagged mutant by confocal microscopy. As reported previously, we found that overexpression of wild-type TICAM-1 in HeLa cells leads to spontaneous activation of TICAM-1 and formation of speckle-like signalosomes (25) (Fig. 4, *upper left panel*). In contrast, the TICAM-1 P434H mutant localized diffusely in the cytosol with slight speckle formation (Fig. 4, *middle left panel*). A fiber-like staining pattern was observed in cells overexpressing the RHIM and N+TIR mutants, which contain the intact TIR domain but not the RHIM domain (*lower left* and *middle right panels*). The double P434H-RHIM mutant also localized diffusely with slight fiber-like formation (*upper right panel*). Finally, overexpression of the dysfunctional N+(TIR-P434H) mutant resulted in a completely diffuse staining pattern (*lower right panel*). These results suggest that Pro^{434} in the TIR domain is a critical for accumulation of TICAM-1 and formation of the fiber-like structures, whereas the RHIM domain is involved in the speckle formation of TICAM-1.

Association of RIP1 and TRAF3 with TICAM-1—To examine the relationship between the reduced activity of the TICAM-1 mutants and changes in their subcellular localization, we analyzed the co-localization of the downstream signaling molecules, RIP1 and TRAF3, with the TICAM-1 mutants by confocal microscopy and immunoprecipitation studies. RIP1 directly associates with TICAM-1 via the RHIM domain leading to activation of NF-κB (14, 15). When HeLa cells were co-transfected with FLAG-tagged RIP1 together with each of the HA-tagged TICAM-1 mutants, we found that RIP1 co-localized with wild-type TICAM-1 and the P434H mutant but not with the RHIM mutant (Fig. 5*A*). The association of RIP1 with these TICAM-1 mutants was confirmed by immunoprecipitation (Fig. 5*B*). As expected, the TICAM-1 mutants containing the mutated RHIM domain (P434H-RHIM) or a deleted C-terminal region (N+TIR) did not interact with RIP1 (data not shown).

Next we analyzed the association of the TICAM-1 mutants with TRAF3, a downstream signaling molecule that is essential for TICAM-1-mediated IRF-3 activation (17, 18). In contrast to RIP1, all of the TICAM-1 mutants with the exception of the dysfunctional N+(TIR-P434H) mutant, co-localized strongly with TRAF3 irrespective of their various localization patterns (Fig. 5*C*). Similar association profiles were observed in the immunoprecipitation studies (Fig. 5*D*), indicating that the mutation of the TIR and RHIM domains barely affected the recruitment of TRAF3. Our data suggest that, once TICAM-1 is oligomerized either through the TIR domain or the C-terminal region, TRAF3 is recruited to the N-terminal region of TICAM-1. Thus, association of TICAM-1 with RIP1 and TRAF3 is necessary but not sufficient for TICAM-1-mediated signaling.

NAP1 and TBK1 Are Recruited to the TICAM-1 Speckle-like Signalosomes—NAP1 has been identified as an essential molecule for TLR3- and RIG-1/MDA-5-mediated IRF-3 activation (16, 23). Because NAP1 directly binds to TBK1, an IRF-3-activating kinase (28), it is possible that NAP1 functions downstream of TRAF3. We examined the localization profile of NAP1 and TBK1 in cells co-expressing the TICAM-1 mutants. Importantly, NAP1 co-localized partially with only wild-type TICAM-1 (Fig. 6*A*). None of the TICAM-1 mutants used in this study co-localized with NAP1 even if the mutants were able to recruit TRAF3 (Fig. 6*A*). In addition, TBK1 also co-localized only with wild-type TICAM-1 (Fig. 6*B*). These results suggest that oligomerization induced by the TIR domain and the

C-terminal region in conjunction with RIP1 binding is required for speckle formation and recruitment of the IRF-3 kinase complexes that lead to effective activation of IRF-3 and NF-κB.

DISCUSSION

TLR3-TICAM-1 signaling results in transcriptional activation of various genes, including the type I IFN and IFN-regulatory genes. In this study, we examined the molecular mecha-

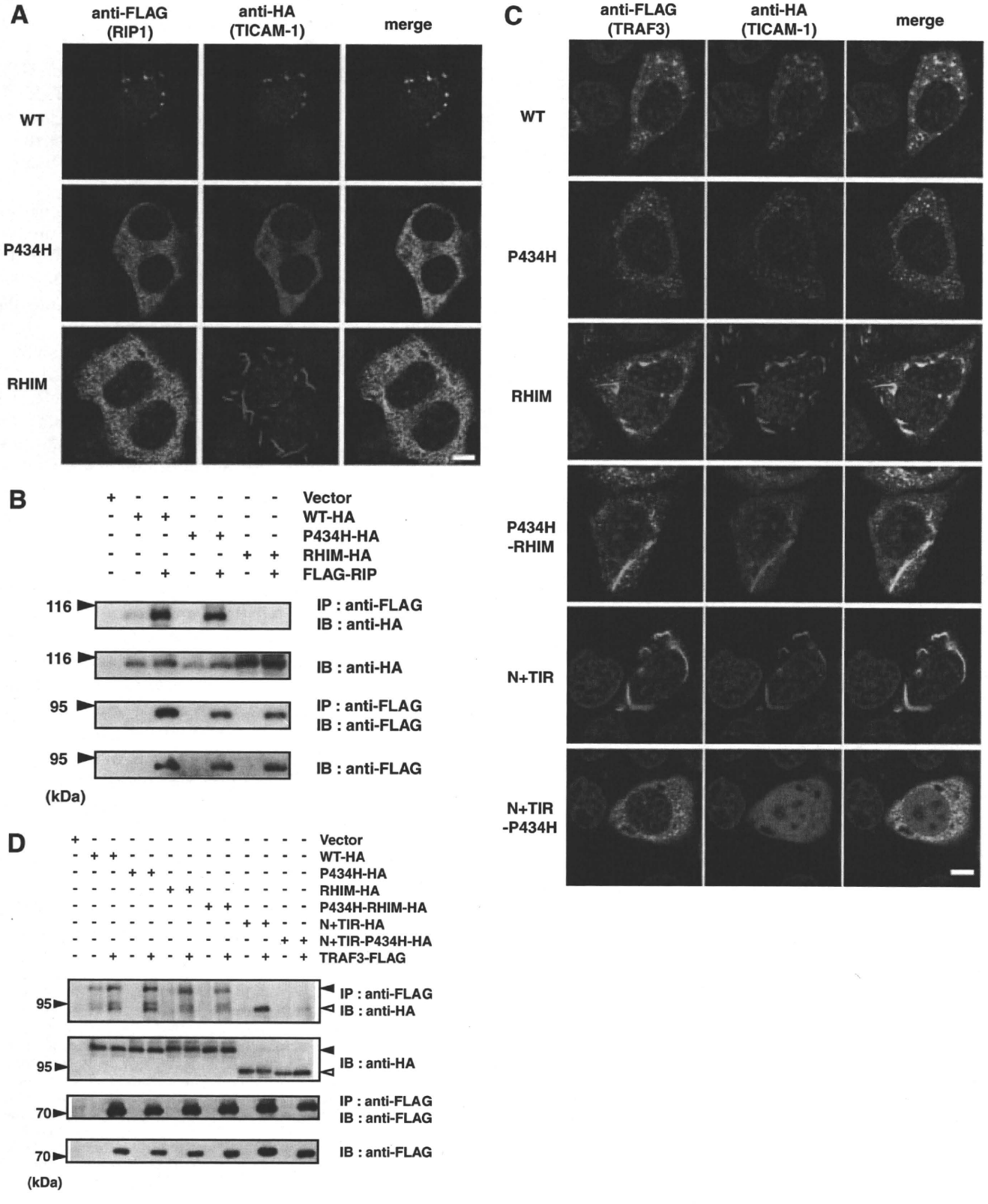

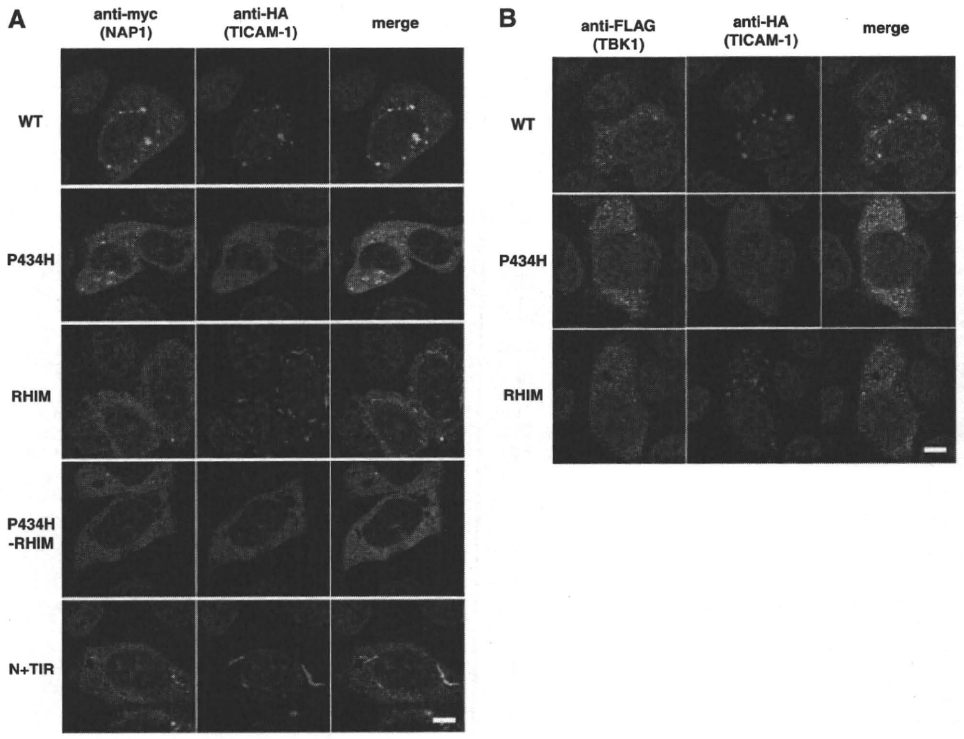

FIGURE 6. **Pro^{434} and the RHIM domain are indispensable for recruitment of NAP1 and TBK1 to TICAM-1.** Confocal images show HeLa cells co-expressing HA-tagged TICAM-1 mutants and Myc-tagged NAP1 (*A*) or FLAG-tagged TBK1 (*B*). *A*, HeLa cells, transfected with the indicated HA-tagged TICAM-1 mutants and Myc-tagged NAP1, were stained with anti-Myc mAb and anti-HA pAb, followed by Alexa488-labeled goat anti-rabbit Ab and Alexa568-labeled goat anti-mouse Ab. *B*, HeLa cells, transfected with the indicated HA-tagged TICAM-1 mutants and FLAG-tagged TBK1, were stained with anti-FLAG mAb and anti-HA pAb, followed by Alexa488-labeled goat anti-rabbit Ab and Alexa568-labeled goat anti-mouse Ab. *Green*, NAP1 (*A*) and TBK1 (*B*); *red*, wild-type and mutated TICAM-1; *blue*, DAPI-stained nuclei. *Bar*, 10 μm.

nism of TICAM-1-mediated signaling and demonstrated that TICAM-1 acts as a platform for recruitment of signaling molecules after homo-oligomerization at the TIR domain and C-terminal region. We show that Pro^{434} in the BB loop of the TIR domain is critical for TICAM-1 homo-oligomerization. Furthermore, the C-terminal region plays an important role in TICAM-1 signaling by inducing homo-dimerization and RIP1 recruitment to the RHIM domain. These results bring new insight into the molecular dynamics of TICAM-1 signaling and regulation of TLR3/4-mediated type I IFN production.

TLR signaling is mediated through TIR-containing adaptor molecules. The conserved proline residue in the BB loop of the TLR-TIR domain is crucial for binding the adaptor molecule (29). The TLR4 mutant P714H fails to bind TICAM-2 resulting in signaling off of TLR4-mediated signaling (9), whereas the dysfunctional TLR3 mutant A795H looses its TICAM-1-recruiting ability (7). Importantly, the TICAM-2-TIR mutant C117H bound the TLR4-TIR but failed to assemble homo (TICAM-2-TICAM-2)- and hetero (TICAM-2-TICAM-1)-dimers (9). Here, we show that Pro^{434} in the TIR domain of TICAM-1 is crucial for mediating interactions with TICAM-1-TIR but not with TLR3-TIR or TICAM-2-TIR. Thus, during TLR3/4-TICAM-1 signaling the BB loop of the upstream TIR determines the association with the downstream TIR domain.

TIR-containing adaptor molecules exhibit different molecular dynamics in response to stimulation by different TLRs. MyD88 is recruited to the plasma membrane or endosome and forms a signaling complex with receptors (30–32). Mal/TIRAP and TICAM-2/TRIF-related adaptor molecule, which associate with the plasma membrane via a phosphatidylinositol 4,5-bisphosphate-binding domain or myristoylation, respectively, act as a sorting adaptor to recruit MyD88 or TICAM-1 (33–35). During TLR4-mediated signaling, TICAM-1 may dissociate from the upstream adaptor TICAM-2 to form speckle-like signalosomes that induce type I IFN as observed during TLR3 signaling (25). Here, we show that TICAM-1 has two homo-dimerization motifs in the TIR domain and the C-terminal region. MyD88 also has the protein-protein interaction domain, the TIR and N-terminal death domain (36). Low molecular weight compounds that disrupt the TIR-TIR interaction of MyD88 have been synthesized to inhibit MyD88 signaling (37, 38). Homo-dimerization motifs of TICAM-1 would be good targets for designing chemical compounds that specifically block TICAM-1 signaling.

Several reports suggest that the C-terminal region of TICAM-1 is important for NF-κB activation and apoptosis in association with RIP1 binding to the RHIM domain but dispensable for IRF-3 activation (14, 15). In our study, decreased

FIGURE 5. **Association of RIP1 and TRAF3 with the TICAM-1 mutants.** *A*, confocal images of HeLa cells co-expressing FLAG-tagged RIP1 and HA-tagged TICAM-1 mutants. Cells were fixed and stained with anti-FLAG mAb and anti-HA pAb, followed by Alexa488-labeled goat anti-rabbit Ab and Alexa568-labeled goat anti-mouse Ab. RIP1 co-localizes with wild-type TICAM-1 and the P434H mutant. *Green*, RIP1; *red*, wild-type and mutated TICAM-1; *blue*, DAPI-stained nuclei. *Bar*, 10 μm. *B*, the RHIM domain of TICAM-1 is essential for association with RIP1. 293FT cells were transfected with the indicated HA-tagged TICAM-1 mutants and FLAG-tagged RIP1. After 24 h, cells were lysed and RIP1 was immunoprecipitated with anti-FLAG mAb. The immunoprecipitants were resolved on SDS-PAGE followed by immunoblotting with anti-HA pAb or anti-FLAG mAb. Total cell lysates were subjected to immunoblotting with anti-HA pAb or anti-FLAG mAb to detect protein expression (*IB*). *C*, confocal images of HeLa cells expressing FLAG-tagged TRAF3 and HA-tagged TICAM-1 mutants. HeLa cells were transfected with the indicated HA-tagged TICAM-1 mutants and FLAG-tagged TRAF3, and then stained with anti-FLAG mAb and anti-HA pAb, followed by Alexa488-labeled goat anti-rabbit Ab and Alexa568-labeled goat anti-mouse Ab. All TICAM-1 mutants except for N+TIR-P434H associate with TRAF3. *Green*, TRAF3; *red*, wild-type and mutated TICAM-1; *blue*, DAPI-stained nuclei. *Bar*, 10 μm. *D*, co-immunoprecipitation of TRAF3 with the TICAM-1 mutants. 293FT cells were transfected with the indicated HA-tagged TICAM-1 mutants and FLAG-tagged TRAF3. After 24 h, cells were lysed and TRAF3 was immunoprecipitated using an anti-FLAG mAb. Samples were resolved on SDS-PAGE followed by immunoblotting with anti-HA Ab or anti-FLAG mAb. Total cell lysates were subjected to immunoblotting with anti-HA pAb or anti-FLAG mAb to detect protein expression (*IB*).

NF-κB and IRF-3 activation was observed in cells overexpressing the TICAM-1 mutants with either a mutated RHIM motif or a deleted C-terminal region compared with cells overexpressing wild-type TICAM-1. These observations are consistent with a previous study using RIP1-deficient cells (39). In the presence of an apoptosis inhibitor, transfection of the same concentration of plasmid resulted in increased protein expression levels of these TICAM-1 mutants compared with wild-type TICAM-1. Why protein expression of the TICAM-1 mutants is higher than that of wild-type TICAM-1 remains question. However, it is possible that wild-type TICAM-1 is rapidly degraded via some protein modifications. RIP1 binding appears to be required for not only NF-κB activation but also IRF-3 activation. Indeed, our immunofluorescence data demonstrate that RIP1 has a critical role in the recruitment of NAP1 and TBK1 to the TICAM-1 speckle-like signalosomes. Because RIP1 associated with the TICAM-1 P434H mutant, it is possible that C-terminal region-mediated homodimerization may trigger RIP1 recruitment.

The TICAM-1 mutant (N+(TIR-P434H)) that lacks both homodimerization motifs failed to homodimerize resulting in abolishment its activity. However, mutants that lacked one homodimerization motif (P434H, P434H-RHIM, and N+TIR) were able to induce homodimerization. Remarkably, these mutants as well as the RHIM mutant recruited TRAF3 but not NAP1 or TBK1. TRAF3 has recently been identified as an essential molecule for TICAM-1-medated IRF-3 activation but not for NF-κB activation (17, 18). Direct interactions between TRAF3 and TICAM-1 were not observed in the yeast two-hybrid system (data not shown). Because TICAM-1 has a TRAF6 binding site at the N-terminal and TRAF2 also directly interacts with the N-terminal region of TICAM-1 (11, 40),[6] TRAF3 appears to form a molecular complex with TICAM-1 via TRAF2/6. In contrast to TRAF3, NAP1 and TBK1 co-localized partially with only wild-type TICAM-1. NAP1 has been identified as a TBK1-binding protein (28) that is involved in the recruitment of TBK1 to the N-terminal region of TICAM-1 (16). Because the TICAM-1 mutants, P434H and RHIM, did not co-localize with NAP1 and TBK1, oligomerization at two different sites in conjunction with RIP1 binding should be required for recruitment of the IRF-3 kinase complex. According to a proteolytic analysis, TICAM-1 possessed the protease-resistant structural domain at the N terminus. This domain was followed by the regions interacted with TRAF6, TRAF2, and TBK1. The TICAM-1 mutant that deleted the structural domain retained full IFN-inducing activity compared with wild-type TICAM-1.[7] One possible explanation why oligomerized TICAM-1 rather than monomer TICAM-1 can recruit downstream molecules is that in the monomer TICAM-1 the region associating with downstream signaling molecules is covered with the N-terminal structural domain. Once TICAM-1 is oligomerized at the TIR and C-terminal domains, the N-terminal region is exposed to interact with downstream molecules. The mechanism of how TICAM-1 recruits the IRF-3 kinase complex requires further investigation. Recent report suggests that TRAF3 ubiquitination facilitates the recruitment of TBK1 (41). We have also observed TICAM-1 phosphorylation and ubiquitination.[6] Structural analysis of the TICAM-1 molecule and characterization of protein modifications of signaling components are important for understanding the molecular topology for initiation of TICAM-1-mediated signaling.

[6] M. Sasai, H. Oshiumi, M. Matsumoto, and T. Seya, manuscript in preparation.
[7] M. Matsumoto, M. Sasai, and T. Seya, unpublished data.

Acknowledgments—We are grateful to M. Shingai, T. Ebihara, A. Ishii, and A. Matsuo for critical discussion. Thanks are also due to Dr. M. Nakanishi (Nagoya City University, Nagoya) and Dr. T. Taniguchi (Tokyo University, Tokyo) for providing plasmids.

REFERENCES

1. Akira, S., Uematsu, S., and Takeuchi, O. (2006) *Cell* **124,** 783–801
2. Yoneyama, M., Kikuchi, M., Natsukawa, T., Shinobu, N., Imaizumi, T., Miyagishi, M., Taira, K., Akira, S., and Fujita, T. (2004) *Nat. Immunol.* **5,** 730–737
3. Alexopoulou, L., Holt, A. C., Medzhitov, R., and Flavell, R. A. (2001) *Nature* **413,** 732–738
4. Matsumoto, M., Kikkawa, S., Kohase, M., Miyake, K., and Seya, T. (2002) *Biochem. Biophys. Res. Commun.* **293,** 1364–1369
5. Schulz, O., Diebold, S. S., Chen, M., Naslund, T. I., Nolte, M. A., Alexopoulou, L., Azuma, Y. T., Flavell, R. A., Liljestrom, P., and Reis e Sousa, C. (2005) *Nature* **433,** 887–892
6. Akazawa, T., Ebihara, T., Okuno, M., Okuda, Y., Shingai, M., Tsujimura, K., Takahashi, T., Ikawa, M., Okabe, M., Inoue, N., Okamoto-Tanaka, M., Ishizaki, H., Miyoshi, J., Matsumoto, M., and Seya, T. (2007) *Proc. Natl. Acad. Sci. U. S. A.* **104,** 252–257
7. Oshiumi, H., Matsumoto, M., Funami, K., Akazawa, T., and Seya, T. (2003) *Nat. Immunol.* **4,** 161–167
8. Yamamoto, M., Sato, S., Hemmi, H., Hoshino, K., Kaisho, T., Sanjo, H., Takeuchi, O., Sugiyama, M., Okabe, M., Takeda, K., and Akira, S. (2003) *Science* **301,** 640–643
9. Oshiumi, H., Sasai, M., Shida, K., Fujita, T., Matsumoto, M., and Seya, T. (2003) *J. Biol. Chem.* **278,** 49751–49762
10. Fitzgerald, K. A., Rowe, D. C., Barnes, B. J., Caffrey, D. R., Visintin, A., Latz, E., Monks, B., Pitha, P. M., and Golenbock, D. T. (2003) *J. Exp. Med.* **198,** 1043–1055
11. Sato, S., Sugiyama, M., Yamamoto, M., Watanabe, Y., Kawai, T., Takeda, K., and Akira, S. (2003) *J. Immunol.* **171,** 4304–4310
12. Sharma, S., tenOever, B. R., Grandvaux, N., Zhou, G. P., Lin, R., and Hiscott, J. (2003) *Science* **300,** 1148–1151
13. Fitzgerald, K. A., McWhirter, S. M., Faia, K. L., Rowe, D. C., Latz, E., Golenbock, D. T., Coyle, A. J., Liao, S. M., and Maniatis, T. (2003) *Nat. Immunol.* **4,** 491–496
14. Meylan, E., Burns, K., Hofmann, K., Blancheteau, V., Martinon, F., Kelliher, M., and Tschopp, J. (2004) *Nat. Immunol.* **5,** 503–507
15. Kaiser, W. J., and Offermann, M. K. (2005) *J. Immunol.* **174,** 4942–4952
16. Sasai, M., Oshiumi, H., Matsumoto, M., Inoue, N., Fujita, F., Nakanishi, M., and Seya, T. (2005) *J. Immunol.* **174,** 27–30
17. Hacker, H., Redecke, V., Blagoev, B., Kratchmarova, I., Hsu, L. C., Wang, G. G., Kamps, M. P., Raz, E., Wagner, H., Hacker, G., Mann, M., and Karin, M. (2006) *Nature* **439,** 204–207
18. Oganesyan, G., Saha, S. K., Guo, B., He, J. Q., Shahangian, A., Zarnegar, B., Perry, A., and Cheng, G. (2006) *Nature* **439,** 208–211
19. Kawai, T., Takahashi, K., Sato, S., Coban, C., Kumar, H., Kato, H., Ishii, K. J., Takeuchi, O., and Akira, S. (2005) *Nat. Immunol.* **6,** 981–988
20. Seth, R. B., Sun, L., Ea, C. K., and Chen, Z. J. (2005) *Cell* **122,** 669–682
21. Meylan, E., Curran, J., Hofmann, K., Moradpour, D., Binder, M., Bartenschlager, R., and Tschopp, J. (2005) *Nature* **437,** 1167–1172
22. Xu, L. G., Wang, Y. Y., Han, K. J., Li, L. Y., Zhai, Z., and Shu, H. B. (2005) *Mol. Cell* **19,** 727–740
23. Sasai, M., Shingai, M., Funami, K., Yoneyama, M., Fujita, T., Matsumoto, M., and Seya, T. (2006) *J. Immunol.* **177,** 8676–8683
24. Saha, S. K., Pietras, E. M., He, J. Q., Kang, J. R., Liu, S. Y., Oganesyan, G.,

Shahangian, A., Zarnegar, B., Shiba, T. L., Wang, Y., and Cheng, G. (2006) *EMBO J.* **25,** 3257–3263
25. Funami, K., Sasai, M., Ohba, Y., Oshiumi, H., Seya, T., and Matsumoto, M. (2007) *J. Immunol.* **179,** 6867–6872
26. Chen, C., and Okayama, H. (1987) *Mol. Cell. Biol.* **7,** 2745–2752
27. Tsujita, T., Tsukada, H., Nakao, M., Oshiumi, H., Matsumoto, M., and Seya, T. (2004) *J. Biol. Chem.* **279,** 48588–48597
28. Fujita, F., Taniguchi, Y., Kato, T., Narita, Y., Furuya, A., Ogawa, T., Sakurai, H., Joh, T., Itoh, M., Delhase, M., Karin, M., and Nakanishi, M. (2003) *Mol. Cell. Biol.* **23,** 7780–7793
29. Xu, Y., Tao, X., Shen, B., Horng, T., Medzhitov, R., Manley, J. L., and Tong, L. (2000) *Nature* **408,** 111–115
30. Latz, E., Visintin, A., Lien, E., Fitzgerald, K. A., Monks, B. G., Kurt-Jones, E. A., Golenbock, D. T., and Espevik, T. (2002) *J. Biol. Chem.* **277,** 47834–47843
31. Latz, E., Schoenemeyer, A., Visintin, A., Fitzgerald, K. A., Monks, B. G., Knetter, C. F., Lien, E., Nilsen, N. J., Espevik, T., and Golenbock, D. T. (2004) *Nat. Immunol.* **5,** 190–198
32. Honda, K., Yanai, H., Mizutani, T., Negishi, H., Shimada, N., Suzuki, N., Ohba, Y., Takaoka, A., Yeh, W. C., and Taniguchi, T. (2004) *Proc. Natl. Acad. Sci. U. S. A.* **101,** 15416–15421
33. Kagan, J. C., and Medzhitov, R. (2006) *Cell* **125,** 943–955
34. Rowe, D. C., McGettrick, A. F., Latz, E., Monks, B. G., Gay, N. J., Yamamoto, M., Akira, S., O'Neill, L. A., Fitzgerald, K. A., and Golenbock, D. T. (2006) *Proc. Natl. Acad. Sci. U. S. A.* **103,** 6299–6304
35. Fitzgerald, K. A., and Chen, Z. J. (2006) *Cell* **125,** 834–836
36. Burns, K., Martinon, F., Esslinger, C., Pahl, H., Schneider, P., Bodmer, J. L., Di Marco, F., French, L., and Tschopp, J. (1998) *J. Biol. Chem.* **273,** 12203–12209
37. Davis, C. N., Mann, E., Behrens, M. M., Gaidarova, S., Rebek, M., Rebek, J., Jr., and Bartfai, T. (2006) *Proc. Natl. Acad. Sci. U. S. A.* **103,** 2953–2958
38. Loiarro, M., Capolunghi, F., Fanto, N., Gallo, G., Campo, S., Arseni, B., Carsetti, R., Carminati, P., De Santis, R., Ruggiero, V., and Sette, C. (2007) *J. Leukoc. Biol.* **82,** 801–810
39. Cusson-Hermance, N., Khurana, S., Lee, T. H., Fitzgerald, K. A., and Kelliher, M. A. (2005) *J. Biol. Chem.* **280,** 36560–36566
40. Jiang, Z., Mak, T. W., Sen, G., and Li, X. (2004) *Proc. Natl. Acad. Sci. U. S. A.* **101,** 3533–3538
41. Kayagaki, N., Phung, Q., Chan, S., Chaudhari, R., Quan, C., O'Rourke, K. M., Eby, M., Pietras, E., Cheng, G., Bazan, J. F., Zhang, Z., Arnott, D., and Dixit, V. M. (2007) *Science* **318,** 1628–1632

THE JOURNAL OF BIOLOGICAL CHEMISTRY VOL. 283, NO. 33, pp. 22787–22794, August 15, 2008

Modulation of Double-stranded RNA Recognition by the N-terminal Histidine-rich Region of the Human Toll-like Receptor 3*[S]

Received for publication, March 24, 2008, and in revised form, May 20, 2008 Published, JBC Papers in Press, June 10, 2008, DOI 10.1074/jbc.M802284200

Kotaro Fukuda[‡1], Tomoya Watanabe[‡], Takashi Tokisue[‡], Tadayuki Tsujita[§], Satoshi Nishikawa[¶], Tsunemi Hasegawa[‡], Tsukasa Seya[§], and Misako Matsumoto[§]

From the [‡]Department of Material and Biological Chemistry, Faculty of Science, Yamagata University, Yamagata 990-8560, Japan, the [§]Department of Microbiology and Immunology, Graduate School of Medicine, Hokkaido University, Kita-ku, Sapporo 060-8638, Japan, and the [¶]Age Dimension Research Center, National Institute of Advanced Industrial Science and Technology, Tsukuba 305-8566, Japan

Toll-like receptors (TLRs) are an essential component of the innate immune response to microbial pathogens. TLR3 is localized in intracellular compartments, such as endosomes, and initiates signals in response to virus-derived double-stranded RNA (dsRNA). The TLR3 ectodomain (ECD), which is implicated in dsRNA recognition, is a horseshoe-shaped solenoid composed of 23 leucine-rich repeats (LRRs). Recent mutagenesis studies on the TLR3 ECD revealed that TLR3 activation depends on a single binding site on the nonglycosylated surface in the C-terminal region, comprising H539 and several asparagines within LRR17 to -20. TLR3 localization within endosomes is required for ligand recognition, suggesting that acidic pH is the driving force for TLR3 ligand binding. To elucidate the pH-dependent binding mechanism of TLR3 at the structural level, we focused on three highly conserved histidine residues clustered at the N-terminal region of the TLR3 ECD: His^{39} in the N-cap region, His^{60} in LRR1, and His^{108} in LRR3. Mutagenesis of these residues showed that His^{39}, His^{60}, and His^{108} were essential for ligand-dependent TLR3 activation in a cell-based assay. Furthermore, dsRNA binding to recombinant TLR3 ECD depended strongly on pH and dsRNA length and was reduced by mutation of His^{39}, His^{60}, and His^{108}, demonstrating that TLR3 signaling is initiated from the endosome through a pH-dependent binding mechanism, and that a second dsRNA binding site exists in the N-terminal region of the TLR3 ECD characteristic solenoid. We propose a novel model for the formation of TLR3 ECD dimers complexed with dsRNA, which incorporates this second binding site.

Mammalian Toll-like receptors (TLRs)[2] play an essential role in the innate immune response to molecular patterns associated with microbial pathogens. To date, more than 10 functional TLRs have been reported in humans and in mice (1). All TLRs are type I integral membrane glycoproteins composed of an ectodomain (ECD) containing varying numbers of leucine-rich repeats (LRRs) linked by a transmembrane domain to a cytoplasmic signaling Toll/IL-1 receptor (TIR) domain. TLR ECDs are responsible for ligand binding; specific ligands derived from bacterial and viral constituents and their respective TLRs have been identified, including lipoteichoic acid (TLR2), lipopolysaccharide (TLR4), flagellin (TLR5), single-stranded RNA (TLR7 and TLR8), and unmethylated CpG DNA motifs (TLR9) (1). The binding of a ligand to a TLR initiates a series of signaling processes that activate and mediate innate and adaptive immune responses (2). The basic mechanism of TLR signaling is thought to involve ligand-induced dimerization (3).

TLR3 is activated by polyinosinic-polycytidylic acid (poly(I:C)), an analog of double-stranded RNA (dsRNA), as well as by viral infection-associated dsRNAs (4). TLR3 is quite distinct from other TLRs in that it is not dependent on myeloid differentiation factor 88 for signaling. Upon ligand binding, the TLR3 TIR domain recruits the intracellular adaptor molecule TICAM-1, also known as TRIF (TIR-containing adaptor inducing IFN-β) (5, 6). The recruitment of this adaptor leads to the production of antiviral cytokines, such as IFN-β. TLR3 is specifically expressed in immune cells, such as conventional dendritic cells and natural killer cells, as well as in fibroblasts and intestinal epithelial cells (1, 7–9).

The crystal structure of the human TLR3 ECD was recently elucidated by two groups (10, 11). The TLR3 ECD is a horseshoe-shaped solenoid composed of 23 LRRs, which is capped on both ends by characteristic N- and C-terminal structures, and its surface is extensively modified with *N*-linked glycans. However, one surface of the LRR solenoid is free from glycosylation, and the charge properties and two loops protruding from LRR12 and LRR20 on this surface are predicted to be involved in TLR3 function. Recent mutagenesis studies on the TLR3 ECD revealed that a single binding site is present on the nonglycosylated surface near the C terminus. This binding site includes His^{539} and several asparagines in LRR17 to -20 and is essential for TLR3 activation, suggesting a model for TLR3 recognition of dsRNA and the formation of a signaling complex (12–14).

* The costs of publication of this article were defrayed in part by the payment of page charges. This article must therefore be hereby marked "*advertisement*" in accordance with 18 U.S.C. Section 1734 solely to indicate this fact.
[S] The on-line version of this article (available at http://www.jbc.org) contains supplemental Tables S1 and S2.
[1] To whom correspondence should be addressed. Tel.: 81-23-628-4580; Fax: 81-23-628-4604; E-mail: kotaro.f@sci.kj.yamagata-u.ac.jp.
[2] The abbreviations used are: TLR, Toll-like receptor; ECD, ectodomain; LRR, leucine-rich repeat; TIR, Toll/interleukin-1 receptor; poly(I:C), polyinosinic-polycytidylic acid; siRNA, small interfering RNA; dsRNA, double-stranded RNA; HEK, human embryonic kidney; QCM, quartz crystal microbalance; MES, 4-morpholineethanesulfonic acid.

Because the inhibition of endosomal acidification abrogates poly(I:C)-driven TLR3 activation, TLR3 is thought to be localized in intracellular compartments, such as endosomes (8). Indeed, a recent report confirmed that TLR3 associates with c-Src tyrosine kinase on endosomes to initiate antiviral signaling (15). It is therefore likely that TLR3, as well as the nucleic acid-recognizing TLRs, TLR7, TLR8 (16), and TLR9 (17), resides in the endosomal membrane and that binding of each TLR to its ligand occurs in the endosomal compartment. The intracellular localization of nucleic acid-sensing TLRs seems to discriminate between self and nonself nucleic acids (18). In addition to this function, several studies have also shown that an acidic pH within endosomes is required for TLR3 recognition of dsRNA and subsequent downstream receptor signaling (13, 19).

To understand the mechanisms underlying TLR3 function and intracellular localization at the structural level, we focused our attention on conformational changes in the receptor ectodomain of TLR3, especially the ionization of histidine side chains. Because one pK_a of histidine is 6.0, protonation of this group within endosomes can generate an ionic attraction to the negatively charged phosphate backbone of dsRNA. If this hypothesis is correct, then the highly conserved histidine residues clustered in the N-terminal region of the TLR3 ECD, namely His^{39} in the N-cap region, His^{60} in LRR1, and His^{108} in LRR3, may play a key role in TLR3 function in acidified endosomes.

Here, we demonstrate that His^{39}, His^{60}, and His^{108} are indeed critical for human TLR3 activation and direct binding to dsRNA. This indicates that, in addition to the C-terminal binding site, there is a second dsRNA binding site in the N-terminal region of the TLR3 ECD characteristic solenoid. Based on these data, we propose a novel model for the formation of TLR3 ECD dimers complexed with dsRNA.

EXPERIMENTAL PROCEDURES

Cell Culture—For the expression of plasmids encoding human TLR3 and its mutants, HEK293 (human embryonic kidney) cells were used and cultured in DMEM cell culture medium (Gibco) supplemented with 10% heat-inactivated fetal bovine serum (Biosource) and antibiotics (penicillin/streptomycin). Sf21 cells used for baculovirus generation and protein expression were grown in suspension culture in Sf-900 II SFM (Gibco) supplemented with 10% heat-inactivated fetal bovine serum (JRH Biosciences) and antibiotics (penicillin/streptomycin and gentamicin).

Plasmids Carrying Wild-type TLR3 and TLR3 ECD—pEFBOS/TLR3, which consists of a human TLR3 cDNA cloned into the mammalian expression vector pEFBOS, was previously described (20). To obtain the recombinant TLR3 ECD protein with the Bac-to-Bac baculovirus expression system (Invitrogen), a construct for the human TLR3 extracellular domain (residues 28–703) was generated by PCR using pEFBOS/TLR3 as a template and a 5′ primer encoding a HindIII site and a 3′ primer encoding a His_6 tag, STOP codon, and HindIII site. The PCR product was cloned into the HindIII site of pFastBac1/rtTLR5S (21), which contains a pFastBac1 donor plasmid backbone, resulting in the construction of pFastBac/TLR3-ECD. The protein expressed from pFastBac/TLR3-ECD contains the preprotrypsin secretion signal sequence and a FLAG tag at the N terminus.

Site-directed Mutagenesis—Mutations were introduced by PCR-mediated, site-directed mutagenesis using essentially the same procedure as described previously (22). Human TLR3 cDNA in pEFBOS/TLR3 was mutated to produce eight mutant plasmids for a reporter gene assay: H39A, H39E, H60A, H60E, H108A, H108E, H539A, and H539E. To generate the four recombinant mutant proteins rH39A, rH60A, rH108A, and rH108E, a cDNA of the human TLR3 ECD in pFastBac/TLR3-ECD was mutated. The mutagenic primers used to mutate human TLR3 are listed in the supplemental materials (Table S1). The mutated DNA sequences were confirmed by sequencing with an Applied Biosystems model 3100A automatic sequencer (Applied Biosystems).

Expression and Purification of Recombinant TLR3 ECD and Its Mutants—Recombinant human TLR3 ECD protein (TLR3-ECD) was obtained using the Bac-to-Bac baculovirus expression system (Invitrogen). To generate the bacmid DNA encoding the TLR3 ECD, *Escherichia coli* DH10Bac cells were transformed with the recombinant donor plasmid pFastBac/TLR3-ECD. The isolated recombinant bacmid DNA was then transfected into Sf21 cells with UniFECTOR (B-Bridge International, San Jose, CA) to generate the recombinant baculoviruses. To express TLR3-ECD, a suspension culture of Sf21 cells in Sf-900 II SFM (Gibco) was infected by the recombinant baculoviruses, and the cell culture supernatant was harvested 5 days after infection. Subsequently, TLR3-ECD was purified using a HiTrap chelating column (5 ml size; GE Healthcare) at 4 °C and analyzed by 8% SDS-PAGE. Protein-containing fractions were pooled and dialyzed in TNE buffer (10 mM Tris-HCl (pH 7.6), 50 mM NaCl, 1 mM EDTA (pH 8.0)). The dialyzed pool was concentrated using YM-50 (Millipore Corp., Bedford, MA), and TLR3-ECD was identified by immunoblotting with both anti-FLAG tag and anti-His_6 tag antibodies. The four recombinant TLR3-ECD mutant proteins (rH39A, rH60A, rH108A, and rH108E) were also expressed and purified by the same procedure. This procedure produced about 50 μg of recombinant protein from 500 ml of culture medium.

RNA and DNA Preparations—For the production of siRNA and $dsRNA_{40}$, two transcription templates were generated by PCR by using two respective sets of primers (Table S2), which contained T7 RNA promoter sequences on each end of the template. Subsequently, siRNA and $dsRNA_{40}$ were transcribed using a T7 AmpliScribe kit (Epicenter Technologies) with [α-^{32}P]CTP. Following *in vitro* transcription, siRNA was prepared according to the instructions for the Silencer siRNA Construction Kit (Ambion). After *in vitro* transcription, annealed $dsRNA_{40}$ was purified in an 8% native polyacrylamide gel. Corresponding, respective sense and antisense strands were used as follows: siRNA, 5′-CCUGUUCCAUGGCCAACACUU-3′ and 5′-GUGUUGGCCAUGGAACAGGUU-3′; $dsRNA_{40}$, 5′-GGGAGACAGGCCUGUUCCAUGGCCAACACGUUUGUCUCCC-3′ and 5′-GGGAGACAAACGUGUUGGCCAUGGAACAGGCCUGUCUCCC-3′. The respective sense and antisense strands of $dsRNA_{48}$, 5′-UCGAGACAGUCACAGUAUCCUCCAGCCUUACAGCCAAGUAUGAGAGCU-3′ and 5′-AGCUCUCAUACUUGGCUGUAAGGCUGGAGGAUACUGUG-

TABLE 1

Analysis of the interaction between TLR3 ECD and nucleic acids under different pH conditions

The binding of TLR3-ECD (20, 50, or 100 nM) to siRNA, $dsRNA_{40}$, $dsRNA_{48}$, rC_{30}, $dsDNA_{40}$, and dC_{30} was evaluated using a filter binding assay as described under "Experimental Procedures." The concentration of ^{32}P-labeled RNA and DNA was 10 nM for each binding reaction. Each value is the mean ± S.D. of three independent experiments. ND, not detected.

TLR3-ECD	Binding					
	siRNA	$dsRNA_{40}$	$dsRNA_{48}$	rC_{30}	$dsDNA_{40}$	dC_{30}
nM	%	%	%	%	%	%
pH 4.2						
20	13 ± 0.3	23 ± 0.8	24 ± 2.4	9.4 ± 0.3	9.2 ± 0.1	3.2 ± 0.8
50	18 ± 0.7	22 ± 2.8	23 ± 2.0	10 ± 0.6	8.4 ± 0.2	4.8 ± 1.0
100	21 ± 1.0	19 ± 2.0	21 ± 0.4	11 ± 1.5	6.9 ± 0.9	5.9 ± 0.3
pH 5.0						
20	2.4 ± 0.6	18 ± 0.9	20 ± 1.0	2.9 ± 0.7	3.8 ± 0.3	2.6 ± 1.0
50	5.7 ± 0.2	19 ± 2.2	22 ± 1.3	5.3 ± 0.1	4.3 ± 0.2	2.3 ± 0.6
100	8.8 ± 0.3	21 ± 3.3	24 ± 0.9	7.1 ± 1.2	5.2 ± 0.1	3.1 ± 0.6
pH 6.0						
20	ND	1.8 ± 0.4	1.7 ± 0.3	ND	ND	1.2 ± 0.4
50	ND	3.4 ± 0.4	5.7 ± 1.9	ND	ND	1.9 ± 0.9
100	ND	8.3 ± 0.7	10 ± 0.1	ND	ND	2.3 ± 0.7
pH 7.6						
20	ND	ND	2.0 ± 0.3	ND	ND	2.2 ± 1.8
50	ND	0.1 ± 0.1	2.7 ± 0.3	ND	ND	1.6 ± 0.3
100	ND	0.2 ± 0.1	3.0 ± 0.3	ND	ND	2.0 ± 0.4

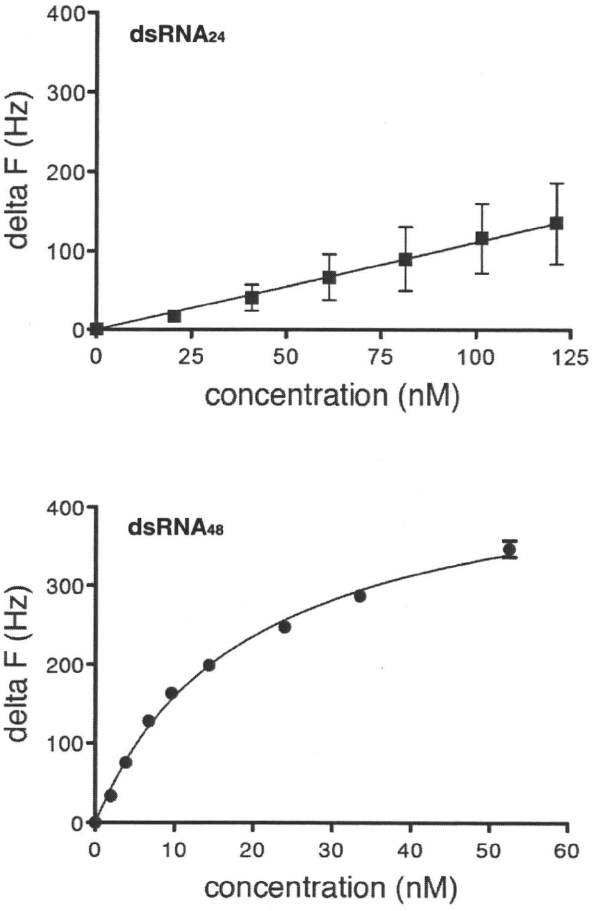

FIGURE 1. **Affinity of TLR3-ECD to $dsRNA_{24}$ and $dsRNA_{48}$.** To investigate the effect of dsRNA length on TLR3 ECD binding at pH 5.0, QCM analysis was performed as described under "Experimental Procedures." TLR3-ECD was injected stepwise into the incubation chamber containing the $dsRNA_{24}$- or $dsRNA_{48}$-coated sensor tip to achieve various concentrations of TLR3-ECD ($dsRNA_{24}$-immobilized QCM, 0–121 nM; $dsRNA_{48}$- immobilized QCM, 0–52.5 nM). The frequency change (*delta F*; Hz) of the dsRNA-immobilized QCM was analyzed, and two binding curves, TLR3-ECD to $dsRNA_{24}$ (*closed squares*) and $dsRNA_{48}$ (*closed circles*), were plotted. Each value is the mean ± S.D. of three independent experiments. The apparent dissociation constant (K_D) calculated for $dsRNA_{48}$ was 19 ± 0.9 nM, but the K_D for $dsRNA_{24}$ could not be determined.

ACUGUCUCGA-3′, were purchased as a duplex RNA from Sigma-Aldrich Japan K.K. The single-stranded RNA of rC_{30} was synthesized using an automated DNA/RNA synthesizer (model 394; ABI). The $dsDNA_{40}$, with a sequence identical to that of $dsRNA_{40}$, was amplified by overlapped-PCR with primers 5′-GGGAGACAGGCCTGTTCCATGGCCA-3′ and 5′-GGGAGACAAACGTGTTGGCCATGGA-3′. The single-stranded DNA of dC_{30} was purchased from Texas Genomics Japan Co. Ltd. All $dsRNA_{48}$, rC_{30}, $dsDNA_{40}$, and dC_{30} were labeled at the 5′-end with [γ-^{32}P]ATP by using T4 polynucleotide kinase.

For the quartz crystal microbalance (QCM) analysis, the respective sense and antisense strands of $dsRNA_{24}$ (5′-end-biotinylated), 5′-CGUAGACAGUCACAGAAUGCUCCA-3′ and 5′-UGGAGCAUUCUGUGACUGUCUACG-3′, and 5′-end-biotinylated $dsRNA_{48}$ were purchased as duplex RNAs from Sigma-Aldrich Japan K.K.

Reporter Gene Assay—HEK293 cells were seeded in 24-well plates (5×10^5 cells/well). Twenty-four hours later, Lipofectamine 2000 (Invitrogen) was used to transiently transfect the cells with pEFBOS/TLR3 or TLR3 mutant expression vectors (0.1 μg) together with a p125-luc reporter (0.1 μg) and a *Renilla* luciferase reporter (0.25 ng). The total amount of transfected plasmid (0.8 μg) was held constant by supplementing with empty vector as needed. Twenty-four hours after transfection, the medium was replaced with fresh medium containing poly(I:C) (10 μg/ml), and the cells were incubated for an additional 6 h. Cells were collected and washed twice with 1 ml of phosphate-buffered saline. The collected cells were lysed using passive lysis buffer (Promega), and the cell lysates were assayed for dual luciferase activities (Promega). Data are expressed as mean relative stimulation ± S.D. for a representative experiment from three independent experiments, performed in triplicate.

Western Blots—HEK293 cells were transiently transfected with target expression vector (0.8 μg) as described above. After 24 h, the cells were collected, washed three times with 1 ml of phosphate-buffered saline, and suspended with lysis buffer (20 mM Tris-HCl (pH 7.4), 150 mM NaCl, 10 mM EDTA (pH 7.4), 1% Nonidet P-40, 25 mM iodoacetamide, 2 mM phenylmethylsulfonyl fluoride) supplemented with Complete Protease Inhibitor (Roche Applied Science). After incubation on ice for 30 min, the lysates were centrifuged, and the supernatants were obtained. The concentration of the supernatants was determined using a protein assay kit (Bio-Rad), and equal amounts of protein were subjected to 7.5% SDS-PAGE. Separated samples were blotted onto polyvinylidene difluoride membrane (Millipore) and probed with a mouse anti-TLR3 antibody (IMG315A; Imegenex Inc.). Horseradish peroxidase-conjugated goat anti-mouse antibody (Biosource) was used as a secondary antibody. Detection of horseradish peroxidase was carried out using a chemiluminescent horseradish peroxidase substrate (Millipore).

Filter Binding Analysis—To analyze the ability of TLR3 to bind siRNA, $dsRNA_{40}$, $dsRNA_{48}$, rC_{30}, $dsDNA_{40}$, and dC_{30},

each ^{32}P-labeled RNA and DNA (10 nM) was incubated with TLR3-ECD (20, 50, or 100 nM) in 50 μl of binding buffer (2 mM HEPES-NaOH (pH 7.6) and 5 mM MES-NaOH (pH 4.2, 5.0, or 6.0) with 100 mM NaCl and 3 mM $MgCl_2$) at 37 °C for 1 h. To evaluate the binding of TLR3-ECD mutants, $dsRNA_{40}$ (10 nM) was incubated with mutants (20 nM) in 50 μl of binding buffer

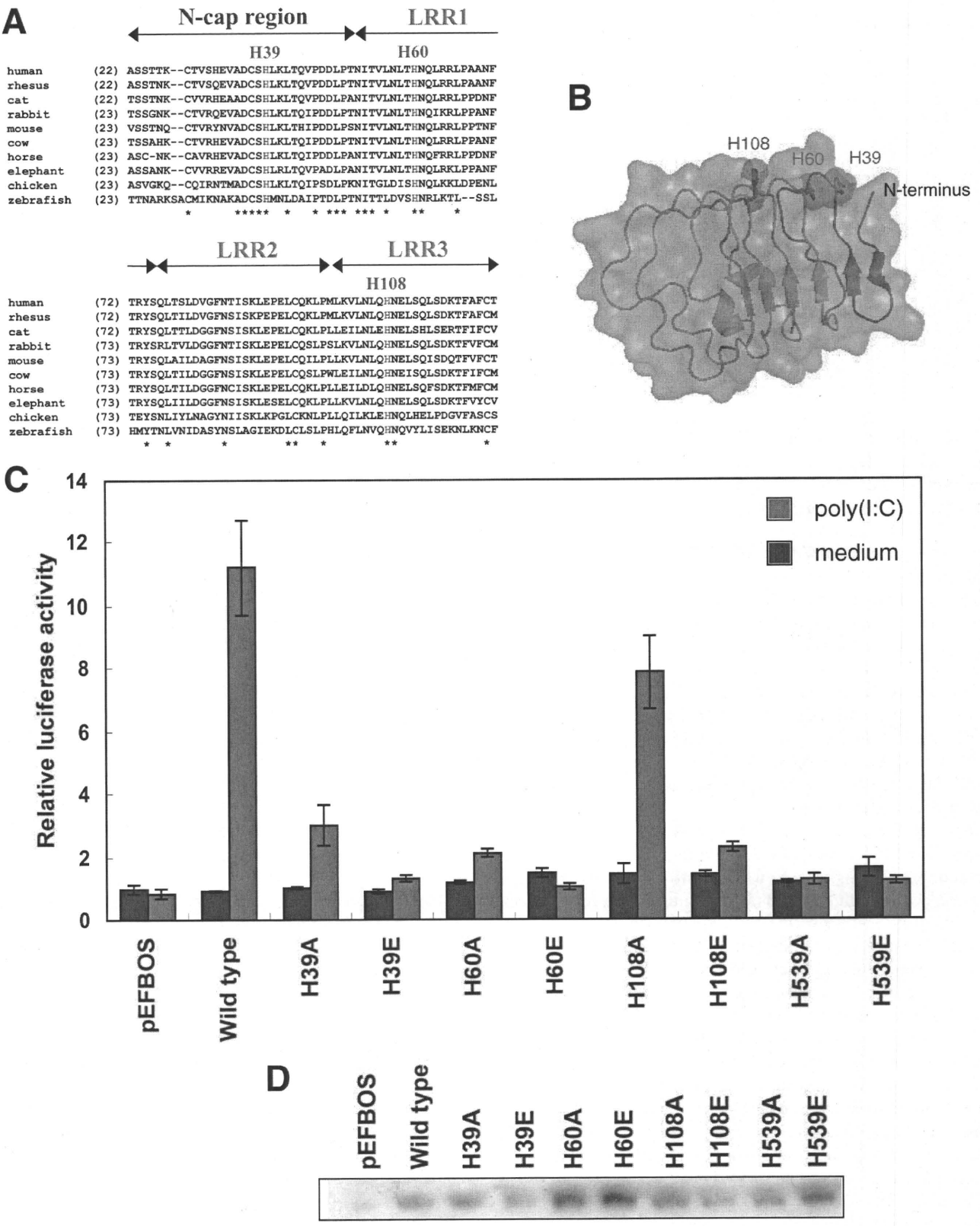

(pH 5.0) as above. The protein-RNA complex was separated by filtration on a nitrocellulose filter (HAWP filter, 0.45 μm; Millipore) fitted in a pop top filter holder (Nucleopore), followed by a wash with 1 ml of binding buffer. Radioactivity remaining on the filter was measured using a BAS2000 image analyzer (Fuji-Film), and the amount of RNA bound to TLR3-ECD or mutants was calculated as a percentage of the RNA input prior to filtration.

QCM Analysis—QCM measurements were performed with a 27-MHz Affinix Q QCM (Initium Co.). The QCM sensor tips were directly immobilized with NeutrAvidin (100 μg/ml; Pierce) in HEPES-NaOH (20 mM, pH 7.6) and NaCl (200 mM) for 12 h at 4 °C. After washing three times with H_2O, the sensor tips were stirred (1000 rpm) at 25 °C in phosphate-buffered saline (1.5 ml) in an incubation chamber. 5′-End biotinylated $dsRNA_{24}$ or $dsRNA_{48}$ (100 pmol) was added to the incubation chamber. To prevent nonspecific interactions between the sensor tip and proteins, phosphate-buffered saline was exchanged with a blocking solution (5 mM MES-NaOH (pH 5.0), 100 mM NaCl, 3 mM $MgCl_2$, and 0.4% Block-Ace Powder (Dainippon Pharma)). TLR3-ECD was then injected stepwise into the incubation chamber containing the immersed dsRNA-coated sensor tip. The binding affinity was indicated by QCM frequency changes recorded by Affinix Q version 1.53 software (Initium), and the disassociation constant (K_D) was calculated with Prism 5 version 5.0a software (Graph Pad Software Inc.).

RESULTS

Importance of Low pH and dsRNA Length for TLR3 ECD Binding—To study the molecular recognition events and biochemical interactions between TLR3 and dsRNA, we first examined the effect of pH on the binding of recombinant TLR3 ECD (TLR3-ECD) to dsRNA. A filter binding assay for TLR3-ECD (20, 50, or 100 nM) was carried out with siRNA, $dsRNA_{40}$, and $dsRNA_{48}$ (10 nM) at pH 4.2–7.6 (Table 1). Binding to TLR3-ECD was undetectable or slight at pH 6.0 and 7.6. However, all dsRNAs bound strongly at lower pH, particularly at pH 4.2. Similar binding patterns were observed for $dsRNA_{40}$ and $dsRNA_{48}$; however, both of these interacted more efficiently with TLR3-ECD than with shorter dsRNA (*i.e.* siRNA).

To examine whether TLR3-ECD could discriminate between single-stranded RNA and dsRNA structures *in vitro*, a filter binding assay was conducted using single-stranded RNA of rC_{30} under the same conditions. Although no detectable binding complex was detected at pH 6.0 or 7.6, binding of rC_{30} at pH 4.2 or 5.0 was moderate compared with the strong binding of $dsRNA_{40}$ (Table 1). Given the preference of TLR3-ECD for dsRNA, the same approach was used to evaluate whether TLR3-ECD could recognize a DNA structure. TLR3-ECD formed a complex with $dsDNA_{40}$, which encoded a sequence identical to that of $dsRNA_{40}$, and the binding was sensitive to pH (Table 1). Although $dsDNA_{40}$ binding was inefficient at pH 6.0 or 7.6, it was moderate at lower pH. Binding of $dsDNA_{40}$ at pH 4.2 and 5.0 was markedly reduced compared with that of $dsRNA_{40}$. The binding of TLR3-ECD to the single-stranded DNA of dC_{30} was much weaker than that to $dsDNA_{40}$ and was not dependent on acidic pH (Table 1). Taken together, these results suggest that the interaction of TLR3-ECD with nucleic acids, especially with dsRNA, is significantly dependent on acidic pH.

We used QCM to more directly characterize the effects of dsRNA length on TLR3 ECD binding in an acidic environment. This highly sensitive QCM technique detects solution phase protein-nucleic acid interactions by monitoring the linear decrease of the emitted frequency, which occurs with increasing mass on the QCM sensor tip. When the $dsRNA_{48}$-coated sensor tip was used, a positive response was observed at all tested concentrations of TLR3-ECD (0–52.5 nM), with an apparent dissociation constant (K_D) of 19 nM (Fig. 1). Strikingly, when the sensor tip was coated with $dsRNA_{24}$ and higher concentrations of TLR3-ECD were used (0–121 nM), the positive response was dramatically reduced, and the K_D value could no longer be determined (Fig. 1). These results suggest that the interaction of TLR3 ECD with dsRNA highly depends on acidic pH and dsRNA length.

His^{39}, His^{60}, and His^{108} Are Essential for the Ligand-dependent Activation of TLR3—To assess how TLR3 senses acidic pH for binding dsRNA, we focused on three highly conserved histidine residues clustered in the N-terminal region of the TLR3 ECD: His^{39} in the N-cap region, His^{60} in LRR1, and His^{108} in LRR3 (Fig. 2*A*). These histidine residues are located between the concave and nonglycosylated lateral surfaces of the TLR3 ECD structure, and all of their imidazole side chains are exposed on the outside of the protein (Fig. 2*B*). Because one pK_a of histidine is 6.0, a pH change within the endosome from neutral to acidic protonates the imidazole group. This is thought to generate an ionic attraction between the histidine and the negatively charged phosphate backbone of the dsRNA.

To test our hypothesis that the N-terminal histidines are crucial for pH-dependent binding of TLR3 ECD to dsRNA, we constructed the site-specific substitution mutants H39A, H39E, H60A, H60E, H108A, and H108E and carried out a reporter gene assay to analyze how mutations in TLR3 influence TLR3 activation. TLR3-negative HEK293 cells were transiently transfected with wild-type (pEFBOS/TLR3) or mutant

FIGURE 2. **His^{39}, His^{60}, and His^{108} mutants affect TLR3 signaling.** *A*, alignment of the N-terminal region of the human TLR3 ECD with homologous sequences from other species. The alignment begins with Ala^{22} of human TLR3. The conserved histidine residues His^{39}, His^{60}, and His^{108}, which were substituted with alanine or glutamic acid in this study, are indicated by *red letters*. *, residues conserved in all 10 species. NCBI accession numbers for sequences are as follows: human, AAH59372; rhesus, NP_001031762; cat, ABB92548; rabbit, ABB76310; mouse, NP_569054; cow, CAH19227; horse, ABB92546; elephant, ABC95781; chicken, ABL74502; zebrafish, NP_001013287. *B*, N-terminal structure of the human TLR3 ECD. The main chain of the N-cap region and the LRR domain are shown with *blue* and *green ribbon models*, respectively. His^{39}, His^{60}, and His^{108}, located on the glycosylation-free face, are represented by *red sticks*. The molecular surface is represented in *gray*, except for His^{39}, His^{60}, and His^{108}, which are in *red* (Protein Data Bank code 2A0Z). *C*, a reporter gene assay was carried out as described under "Experimental Procedures." HEK293 cells transfected with wild-type or mutant TLR3 were (*red bars*) or were not (*blue bars*) stimulated with 10 μg/ml of poly(I:C). Firefly luciferase activity was normalized to *Renilla* luciferase activity. Relative luciferase units were calculated by dividing the normalized luciferase activity by the result obtained using unstimulated, empty pEFBOS vector. *D*, expression of the wild-type and TLR3 mutants was confirmed by Western blotting as described under "Experimental Procedures." The Western blot was probed with mouse anti-TLR3 antibody IMG315A.

TLR3 expression plasmids together with a reporter plasmid containing a luciferase gene under the control of the human IFN-β promoter; the cells were then stimulated with poly(I:C).

Although H108A failed to substantially abrogate the TLR3-mediated activation of luciferase activity, the H39A, H39E, H60A, H60E, and H108E mutants showed a nearly complete loss of function (Fig. 2*C*). The replacement of the histidine residues with glutamic acid rather than alanine had a stronger effect on TLR3 activation by poly(I:C), especially for His^{108}. This may be due to the ionic repulsion between the glutamic acid introduced at His^{39}, His^{60}, and His^{108} and the negative charge on the phosphate backbone of the dsRNA. The mutants did not regain activity, even when 5-fold higher concentrations of the mutant TLR3 expression plasmids were employed (data not shown). This loss of activity was not due to low expression, since Western blot analysis showed that the expression level of each mutant protein was equal to or greater than that of the wild-type (Fig. 2*D*). Thus, His^{39}, His^{60}, and His^{108} in the N-terminal region of the TLR3 ECD are essential for ligand-dependent activation of TLR3.

Direct Binding between His^{39}, His^{60}, and His^{108} and dsRNA—To elucidate whether these essential histidine residues directly contacted dsRNA, we analyzed the binding between recombinant mutant TLR3 proteins and $dsRNA_{40}$ at acidic pH. Purified TLR3-ECD mutant proteins, rH39A, rH60A, rH108A, and rH108E, were verified by performing 8% SDS-PAGE stained with Coomassie Blue R-250 (Fig. 3*A*). rH108A showed partial loss of binding (about 60% of the wild type) to $dsRNA_{40}$ at pH 5.0 (Fig. 3*C*). In contrast, rH39A, rH60A, and rH108E exhibited remarkably diminished binding to $dsRNA_{40}$ (Fig. 3, *B* and *C*). These observations clearly correlated with the results obtained in the reporter gene assay (Fig. 2*C*). It can therefore be concluded that the loss of function observed in the TLR3 mutants is due to their inability to recognize dsRNA and that His^{39}, His^{60}, and His^{108} are essential for the direct binding of TLR3 to dsRNA at acidic pH.

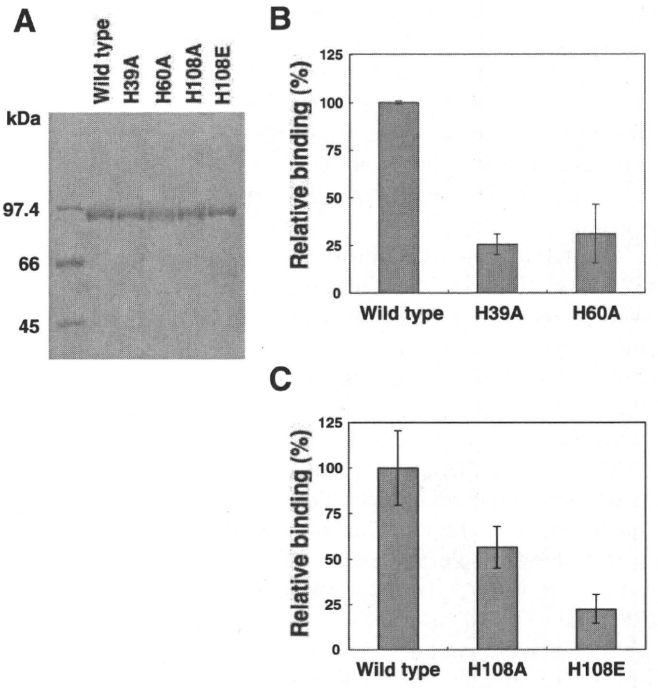

FIGURE 3. **Binding of TLR3-ECD mutants to $dsRNA_{40}$.** *A*, purified TLR3-ECD mutant proteins. Approximately 0.5 μg of wild type and each of the mutant proteins, rH39A, rH60A, rH108A, and rH108E, were loaded on an 8% SDS-PAGE. *B* and *C*, to analyze the binding of TLR3-ECD mutants, ^{32}P-labeled $dsRNA_{40}$ (10 nM) was incubated with TLR3-ECD (wild type), rH39A, rH60A, rH108A, or rH108E (20 nM) in 50 μl of binding buffer (5 mM MES-NaOH (pH 5.0), 100 mM NaCl, and 3 mM $MgCl_2$) at 37 °C for 1 h. A filter binding assay was carried out as described under "Experimental Procedures." To normalize the data, wild-type binding activity was set to 100%. The values ± S.D. are derived from three independent experiments.

DISCUSSION

Mutational analyses have identified several important residues in the TLR3 ECD that are essential for ligand recognition and signal transduction. An impressive report by Bell *et al.* (12) showed that His^{539} and Asn^{541} in LRR20 are crucial for the activation of TLR3. Following this report, Ranjith-Kumar *et al.* (13) identified asparagines in LRR17 to LRR20 that also contribute to TLR3 activation. In this study, we identified three histidine residues, His^{39} in the N-cap region, His^{60} in LRR1, and His^{108} in LRR3, that are essential for human TLR3 activation and ligand binding. In contrast with our results, Bell *et al.* (12) reported that H39A and H60A had no effect on TLR3 activation. This discrepancy may be due to sensitivity differences in the cell-based assay systems used, as observed for the His^{539} substitution mutants. According to their report, the H539E mutation, but not the H539A mutation, resulted in almost complete loss of function. However, in our assay system, both H539E and H539A showed significant effects on TLR3 activation (Fig. 2*C*).

Because $dsRNA_{40}$ was bound to TLR3-ECD more efficiently than to the same sequence of $dsDNA_{40}$, we posit that there exists a difference between forms of dsRNA (A-DNA-like form) and dsDNA (B-form) with respect to nucleic acid backbone helical structures and/or recognition of the 2′-OH group in the ribose of dsRNA (Table 1). Indeed, it has been reported that the presence of the ribose 2′-OH group in poly(I:C) is essential for its recognition by TLR3 (20). Furthermore, the efficiency of TLR3-ECD binding to dsRNA was strictly modulated by the acidic pH conditions, as shown in Table 1. These results indicate that His^{539} and the histidine cluster at the N-terminal region might act as pH sensors to recruit dsRNA. Once the imidazole side chains are protonated in an acidic compartment, such as an endosome, the resulting positive electrostatic potential would presumably lead to the interaction of TLR3 with dsRNA. This suggests that TLR3 signaling is initiated from within the endosome, based on a pH-dependent binding mechanism that is regulated by these functional histidine residues. Consistent with this, Ranjith-Kumar *et al.* (13) previously reported observations from a UV cross-linking assay showing that the TLR3 ECD specifically interacts with dsRNA at acidic pH. Furthermore, Bouteiller *et al.* (19) have shown using a chimeric TLR3-CD32 receptor that recognition of dsRNA by TLR3 and subsequent signal transduction require an acidic pH. It is therefore likely that TLR3-dsRNA interactions occur in acidic compartments to activate signal transduction. Histidine residues on other receptors have also been implicated in acid-regulated mechanisms (23, 24). Other nucleic acid-recognizing TLRs, TLR7, TLR8, and TLR9, are localized in acidic compart-

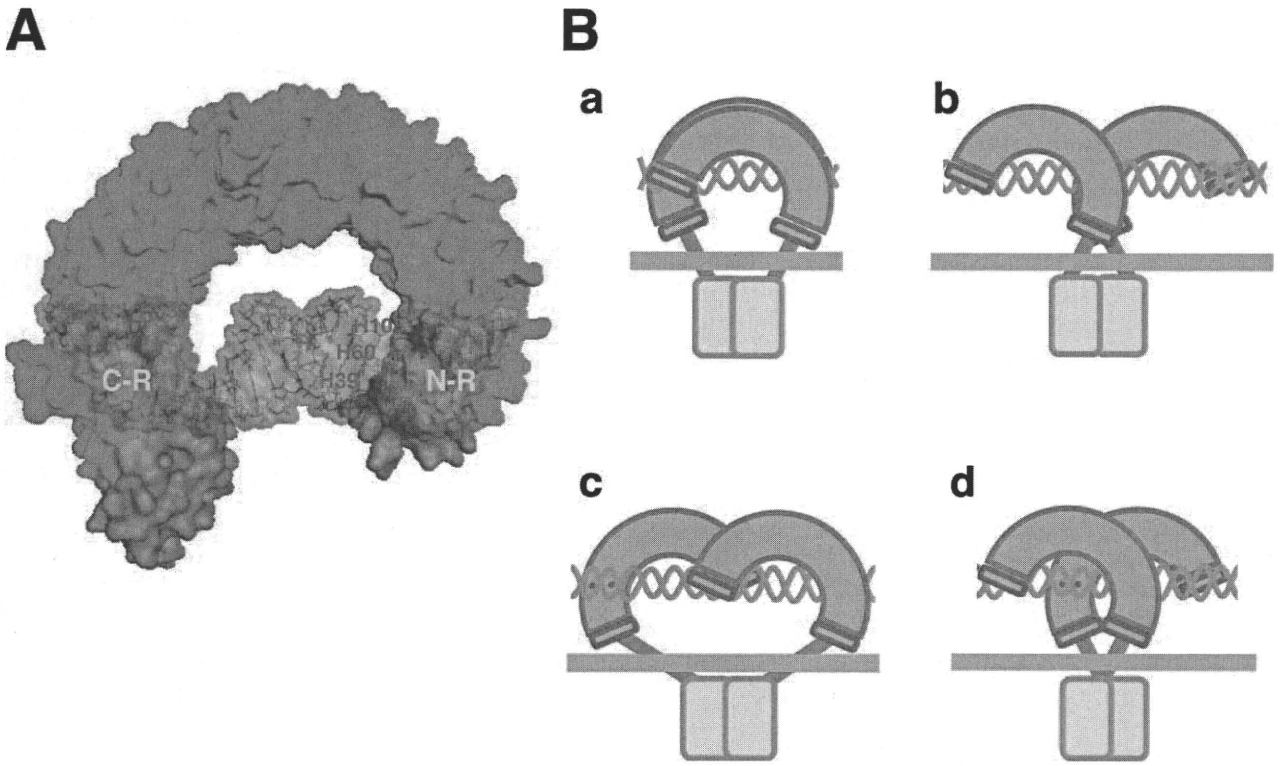

FIGURE 4. **Model of TLR3 ECD recognition of dsRNA and formation of symmetric TLR3 dimers.** *A*, the N-cap region, C-cap region, and LRR domain are represented by *blue*, *magenta*, and *green* surfaces, respectively (Protein Data Bank code 2A0Z). His^{39}, His^{60}, and His^{108} in the N-terminal region (*N-R*) and His^{539} and Asn^{541} in the C-terminal region (*C-R*) are shown in *red* and are involved in the interaction with a dsRNA, 29 bp in length (*gray surface*; Protein Data Bank code 1QC0). Using manual docking performed with PyMOL (version 0.99, DeLano Scientific LLC), we determined that a 29-bp dsRNA can lie across both the N-terminal region and C-terminal region in the TLR3 ECD solenoid and that the minor groove provides the interaction surface for His^{39}, His^{60}, and His^{108}. The interval between the two binding sites is estimated to be two helical turns of dsRNA. *B*, a dsRNA cross-links two molecules of the TLR3 ECD, related by a 180° rotation, resulting in a precisely symmetrical dimer of the TLR3 ECD. Two TLR3 ECD molecules sandwich a dsRNA at two sites in both the N-terminal region and C-terminal region, fixing the dsRNA at four sites. Because the symmetrical arrangement of two TLR3 ECD molecules can be changed by sliding along a dsRNA, it is difficult to determine a single, accurate signaling complex. Two TLR3 ECD molecules can sandwich a dsRNA in both the N-terminal region and C-terminal region (*a*), only the C-terminal region (*b*), or only the N-terminal region (*c*). *d*, the dsRNA is not sandwiched between the N-terminal region or the C-terminal region. The *color scheme* is the same as in *A*. The *yellow boxes* represent the TIR domains.

ments, such as endosomes, indicating that the ligand-binding and signaling of these receptors are also likely to require acidic pH. Indeed, it has been reported that TLR9 interacts with its ligand, nonmethylated CpG DNA, at acidic pH (25).

The basic mechanism of TLR signaling is thought to involve ligand-induced dimerization. In a model proposed by Bell *et al.* (12), the TLR3 ECD contains a single ligand-binding site in LRR20 close to the C terminus, and two TLR3 monomers sandwich a dsRNA in a precisely symmetrical arrangement. Ranjith-Kumar *et al.* (13) proposed a similar architecture for TLR3 ECD complexed with dsRNA, although they suggested a model different from that of Bell *et al.* (12), in which ligand binding to the TLR3 ECD induces dimerization and subsequent TIR domain activation. In this study, we revealed a second histidine-enriched binding site in the N-terminal region of the TLR3 ECD, in addition to the limited C-terminal binding site. We also found that the binding constant of $dsRNA_{24}$ was much higher than that of $dsRNA_{48}$ (Fig. 1). This indicates that the stability of the TLR3-dsRNA complex is affected by the dsRNA length. Although the 24-bp length of dsRNA would be sufficient for TLR3 binding if the ECD contained only the limited C-terminal binding site, the binding constants indicate that $dsRNA_{24}$ affinity for TLR3-ECD is quite low compared with that of $dsRNA_{48}$. Given the approximate distance between the N- and C-terminal binding sites (~30 bp of dsRNA; *gray surface* in Fig. 4*A*), $dsRNA_{48}$, but not $dsRNA_{24}$, is sufficiently long to bridge the distance between the regions. These results, together with the recent report that TLR3 ECD monomers bind cooperatively to dsRNA to form stable dimeric complexes and require a dsRNA length of at least 40–50 bp to bind a single dimmer (26), strongly suggest that there exist two binding sites in the TLR3 ECD, which are both essential for the dsRNA recognition by the TLR3 ECD.

Taking into account all of these data, we determined that a 29-bp length of dsRNA (Fig. 4*A*, *gray surface*) can lie across the two binding sites on the TLR3 solenoid, based on configuration adaptability predicted by a manual docking analysis (Fig. 4*A*). From this analysis, we propose a new model for the formation of symmetric TLR3 dimers (Fig. 4*B*). Given that the N- and C-terminal binding sites appear on the same glycosylation-free face, it would be possible to assemble at least four ternary architectural units, each composed of two TLR3s and a single dsRNA (Fig. 4*B*). A commonly observed feature is that two TLR3 monomers contact a dsRNA via two N- and C-terminal binding sites, so that a dsRNA is fixed at four different positions in a single unit. Although the capability to form dimers in the TIR domain is vital for subsequent signaling, the symmetric arrangement of the two TLR3 molecules can vary along the

length of a dsRNA (see the legend to Fig. 4*B*). Communication between the two nonglycosylated faces of the TLR3 ECD separated by the dsRNA (*e.g.* the loop structure protruding from LRR12), might determine the exact structure of the dimer. Further biochemical analyses or determination of the crystal structure of TLR3 ECD in complex with a dsRNA will be required to determine the precise mechanism by which TLR3 recognizes dsRNA.

Our study with single amino acid mutations in TLR3 demonstrates that the histidine cluster in the N-terminal region functions to recognize dsRNA based on acid-regulated mechanisms, indicating the presence of a second dsRNA binding site in the characteristic solenoid of the TLR3 ECD. This finding has led us to propose a novel dimer structure, which provides insight into the ligand recognition mechanism of TLR3.

Acknowledgments—We thank K. Ito, K. Funami, and E. Takada (Hokkaido University) for technical support with the cell-based experiments. We thank T. Jitsukawa and S. Chiba (ULVAC, Inc.) for technical support with the QCM analysis. We thank F. Nishikawa (AIST) for the preparation of rC_{30}. We also thank S. Miyata, Y. Asanuma, K. Hatakeyama, K. Konno, R. Narita, and R. Tozuka (Yamagata University) for technical support with the construction of wild-type and mutant TLR3 expression plasmids.

REFERENCES

1. Akira, S., Uematsu, S., and Takeuchi, O. (2006) *Cell* **124,** 783–801
2. Iwasaki, A., and Medzhitov, R. (2004) *Nat. Immunol.* **5,** 987–995
3. Gay, N. J., Gangloff, M., and Weber, A. N. (2006) *Nat. Rev. Immunol.* **6,** 693–698
4. Alexopoulou, L., Holt, A. C., Medzhitov, R., and Flavell, R. A. (2001) *Nature* **413,** 732–738
5. Oshiumi, H., Matsumoto, M., Funami, K., Akazawa, T., and Seya, T. (2003) *Nat. Immunol.* **4,** 161–167
6. Yamamoto, M., Sato, S., Mori, K., Hoshino, K., Takeuchi, O., Takeda, K., and Akira, S. (2002) *J. Immunol.* **169,** 6668–6672
7. Matsumoto, M., Kikkawa, S., Kohase, M., Miyake, K., and Seya, T. (2002) *Biochem. Biophys. Res. Commun.* **293,** 1364–1369
8. Matsumoto, M., Funami, K., Tanabe, M., Oshiumi, H., Shingai, M., Seto, Y., Yamamoto, A., and Seya, T. (2003) *J. Immunol.* **171,** 3154–3162
9. Schroder, M., and Bowie, A. G. (2005) *Trends Immunol.* **26,** 462–468
10. Choe, J., Kelker, M. S., and Wilson, I. A. (2005) *Science* **309,** 581–585
11. Bell, J. K., Botos, I., Hall, P. R., Askins, J., Shiloach, J., Segal, D. M., and Davies, D. R. (2005) *Proc. Natl. Acad. Sci. U. S. A.* **102,** 10976–10980
12. Bell, J. K., Askins, J., Hall, P. R., Davies, D. R., and Segal, D. M. (2006) *Proc. Natl. Acad. Sci. U. S. A.* **103,** 8792–8797
13. Ranjith-Kumar, C. T., Miller, W., Xiong, J., Russell, W. K., Lamb, R., Santos, J., Duffy, K. E., Cleveland, L., Park, M., Bhardwaj, K., Wu, Z., Russell, D. H., Sarisky, R. T., Mbow, M. L., and Kao, C. C. (2007) *J. Biol. Chem.* **282,** 7668–7678
14. Takada, E., Okahira, S., Sasai, M., Funami, K., Seya, T., and Matsumoto, M. (2007) *Mol. Immunol.* **44,** 3633–3640
15. Johnsen, I. B., Nguyen, T. T., Ringdal, M., Tryggestad, A. M., Bakke, O., Lien, E., Espevik, T., and Anthonsen, M. W. (2006) *EMBO J.* **25,** 3335–3346
16. Gibbard, R. J., Morley, P. J., and Gay, N. J. (2006) *J. Biol. Chem.* **281,** 27503–27511
17. Latz, E., Schoenemeyer, A., Visintin, A., Fitzgerald, K. A., Monks, B. G., Knetter, C. F., Lien, E., Nilsen, N. J., Espevik, T., and Golenbock, D. T. (2004) *Nat. Immunol.* **5,** 190–198
18. Barton, G. M., Kagan, J. C., and Medzhitov, R. (2006) *Nat. Immunol.* **7,** 49–56
19. de Bouteiller, O., Merck, E., Hasan, U. A., Hubac, S., Benguigui, B., Trinchieri, G., Bates, E. E., and Caux, C. (2005) *J. Biol. Chem.* **280,** 38133–38145
20. Okahira, S., Nishikawa, F., Nishikawa, S., Akazawa, T., Seya, T., and Matsumoto, M. (2005) *DNA Cell Biol.* **24,** 614–623
21. Tsujita, T., Tsukada, H., Nakao, M., Oshiumi, H., Matsumoto, M., and Seya, T. (2004) *J. Biol. Chem.* **279,** 48588–48597
22. Fukuda, K., Morioka, H., Imajou, S., Ikeda, S., Ohtsuka, E., and Tsurimoto, T. (1995) *J. Biol. Chem.* **270,** 22527–22534
23. Rudenko, G., Henry, L., Henderson, K., Ichtchenko, K., Brown, M. S., Goldstein, J. L., and Deisenhofer, J. (2002) *Science* **298,** 2353–2358
24. Doi, T., Kurasawa, M., Higashino, K., Imanishi, T., Mori, T., Naito, M., Takahashi, K., Kawabe, Y., Wada, Y., Matsumoto, A., and Kodama, T. (1994) *J. Biol. Chem.* **269,** 25598–25604
25. Rutz, M., Metzger, J., Gellert, T., Luppa, P., Lipford, G. B., Wagner, H., and Bauer, S. (2004) *Eur. J. Immunol.* **34,** 2541–2550
26. Leonard, J. N., Ghirlando, R., Askins, J., Bell, J. K., Margulies, D. H., Davies, D. R., and Segal, D. M. (2008) *Proc. Natl. Acad. Sci. U. S. A.* **105,** 258–263

Molecular Immunology 45 (2008) 2734–2742

Contents lists available at ScienceDirect

Molecular Immunology

journal homepage: www.elsevier.com/locate/molimm

Selective synergy in anti-inflammatory cytokine production upon cooperated signaling via TLR4 and TLR2 in murine conventional dendritic cells

Noriyuki Hirata[a], Yoshiki Yanagawa[a], Takashi Ebihara[b], Tsukasa Seya[b], Satoshi Uematsu[c], Shizuo Akira[c], Fumie Hayashi[a], Kazuya Iwabuchi[a], Kazunori Onoé[a,*]

[a] Division of Immunobiology, Institute for Genetic Medicine, Hokkaido University, Kita-15, Nishi-7, Kita-ku, Sapporo 060-0815, Japan
[b] Department of Microbiology and Immunology, Graduate School of Medicine, Hokkaido University, Sapporo, Japan
[c] Department of Host Defense, Research Institute for Microbial Diseases, Osaka University, Osaka, Japan

ARTICLE INFO

Article history:
Received 26 December 2007
Accepted 13 February 2008
Available online 26 March 2008

Keywords:
Dendritic cells
Toll-like receptor
Cytokines
Signal transduction

ABSTRACT

Toll-like receptor (TLR) ligands, i.e. lipopolysaccharide (LPS), induce dendritic cell (DC) production of both inflammatory and anti-inflammatory cytokines including interleukin (IL)-12, tumor necrosis factor (TNF)-α, and IL-10. The balance of inflammatory versus anti-inflammatory cytokines appears to be crucial to control immune homeostasis. In the present study, we investigated TLR-mediated regulation of inflammatory versus anti-inflammatory cytokine production using murine bone marrow derived conventional DCs. Standard LPS (sLPS) that contains lipoprotein, a TLR2 ligand, induced vigorous production of both IL-10 and IL-12 p40 by DCs. Highly purified LPS (ultra-pure LPS, upLPS) also induced vigorous production of IL-12 p40, but markedly low IL-10 production. Thus, signal deficiency through TLR2 appeared to result in marked reduction in DC production of IL-10 but not IL-12 p40 upon stimulation with upLPS. To examine this possibility, DCs were stimulated with Pam3CSK4, a synthetic ligand of TLR2, in addition to stimulation with upLPS. It was shown that Pam3CSK4 alone failed to induce IL-10 production. However, Pam3CSK4 synergistically enhanced upLPS-induced DC production of IL-10 but neither IL-12 p40 nor TNF-α. Extracellular signal-regulated kinase (ERK)1/2, p38 mitogen-activated protein kinase (MAPK), and c-jun N-terminal kinase (JNK)1/2 in DCs were significantly activated by upLPS stimulation. The upLPS-induced activities of these MAPKs were considerably enhanced by additional stimulation with Pam3CSK4. Blocking either p38 MAPK or JNK1/2 pathway completely inhibited the synergistic enhancement of the IL-10 production by DCs upon upLPS and Pam3CSK4 stimulation. Thus, cooperated stimulation of these MAPKs via TLR4 and TLR2 appeared to induce selective synergy in anti-inflammatory cytokine production by murine conventional DCs.

1. Introduction

Toll-like receptors (TLRs) are pattern recognition receptors that recognize pathogen-associated molecular patterns in the pathogen-derived molecules and induce innate immune responses. Lipopolysaccharide (LPS) is a major structural component of Gram-negative bacteria and potently activates monocyte/macrophages and dendritic cells (DCs) (Miller et al., 2005). LPS is recognized by TLR4 expressed on these cells and induces vigorous productions of various cytokines (Fujihara et al., 2003; Miller et al., 2005). Like the other TLRs, the cytoplasmic tail of TLR4 contains a Toll-IL-1R (TIR) domain (Imler and Hoffmann, 2003; O'Neill and Bowie, 2007). Upon TLR4 activation, TIR domain efficiently recruits several TIR-containing intracellular adaptor proteins including myeloid differentiation primary-response gene 88 (MyD88) (Medzhitov et al., 1998; Akira et al., 2001) and TIR domain-containing adaptor inducing IFN-β (TRIF) (Fitzgerald et al., 2001; Horng et al., 2001). The MyD88-dependent signaling pathway activates mitogen-activated protein kinases (MAPKs), nuclear factor-κB (NF-κB), activator protein-1 (AP-1), and interferon regulatory factor (IRF) 5 via TNF receptor-associated factor (TRAF) 6, which induces inflammatory cytokine synthesis. The TRIF-dependent signaling pathway activates IRF3, IRF7 and delayed NF-κB via receptor interacting protein (RIP) 1, TRAF3 and TRAF6, which induces type I interferons (IFNs) (Covert et al., 2005; O'Neill and Bowie, 2007; Kawai and Akira, 2007).

DCs are potent antigen-presenting cells (APCs) and play major roles in the initiation and the regulation of acquired immune responses to various pathogenic antigens (Steinman, 1991; Hart, 1997; Banchereau and Steinman, 1998). LPS-activated DCs produce a large amount of inflammatory cytokines including tumor necrosis factor (TNF)-α, interleukin (IL)-1, IL-6, and IL-12, and also

* Corresponding author. Tel.: +81 11 706 5532; fax: +81 11 706 7545.
E-mail address: kazunori@igm.hokudai.ac.jp (K. Onoé).

0161-5890/$ – see front matter © 2008 Elsevier Ltd. All rights reserved.
doi:10.1016/j.molimm.2008.02.010

anti-inflammatory cytokines including IL-10. DC-produced IL-12 drives polarization of naïve $CD4^+$ T cells toward Th1, while the IL-10 is involved in inhibition of Th1 responses and differentiation of regulatory T cells (McGuirk and Mills, 2002; Rutella et al., 2006; Belkaid, 2007; O'Garra and Vieira, 2007). Thus, the balance of inflammatory versus anti-inflammatory cytokines produced by DCs appears to be crucial to control immune homeostasis. However, mechanism underlying the regulation of the cytokine balance has not been fully understood in DCs.

Although widely used standard LPS (sLPS) are generally contaminated with other bacterial components such as lipoproteins that activate TLR2-mediated signaling (Hirschfeld et al., 2000; Tapping et al., 2000; Hellman et al., 2003), precise influence of these components on DC functions is not well characterized. In the present study, we compared effects of sLPS and ultra-pure LPS (upLPS) that activates only TLR4-mediated pathway on inflammatory and anti-inflammatory cytokine production by murine bone marrow derived conventional DCs (BMDCs). In addition, we examined effect of simultaneous DC stimulation with upLPS and Pam3CSK4 (P3C), a synthetic ligand for TLR2, on the cytokine production. We show herein that cooperated signals via TLR4 and TLR2 induce synergistic production of anti-inflammatory cytokine, IL-10, but not inflammatory cytokines, IL-12 p40 and TNF-α, in murine conventional DCs.

2. Materials and methods

2.1. Reagents and antibodies (Abs)

Murine recombinant granulocyte–macrophage colony-stimulating factor (GM-CSF) was purchased from PeproTech (Rocky Hill, NJ). Low Tox-M Rabbit Complement was purchased from Cedarlane (Ontario, Canada). Standard LPS (sLPS) from *Escherichia coli* (O55:B5) was obtained from Sigma–Aldrich (St. Louis, MO). Ultra-pure LPS (upLPS) from *E. coli* (O111:B4) and Pam3CSK4 (P3C), a synthetic lipopeptide, were purchased from Invivogen (San Diego, CA). Fluorescein isothiocyanate (FITC)-conjugated anti-mouse CD86 monoclonal Ab (mAb) (GL1), phycoerythrin (PE)-conjugated anti-mouse CD40 mAb (3/23), biotin-conjugated anti-I-A^b mAb (AF6-120.1), and streptavidin-peridinin chlorophyll protein (PerCP) were obtained from BD Pharmingen (San Jose, CA). Anti-phospho-p44/42 MAPK (pERK1/2) (Thr^{202}/Tyr^{204}) Ab, anti-phospho-p38 MAPK (Thr^{180}/Thr^{182}) Ab, anti-phospho-SAPK/JNK (pJNK1/2) (Thr^{183}/Tyr^{185}) Ab, anti-phospho-NF-κB p65 (Ser^{536}) Ab, horseradish-peroxidase (HRP)-conjugated anti-rabbit IgG Ab, and HRP-conjugated anti-mouse IgG Ab were purchased from Cell Signaling Technology (Beverly, MA). U0126, a specific inhibitor of mitogen-activated protein kinase/extracellular signal-regulated kinase (MEK)1/2, SB203580, a specific inhibitor of p38 MAPK, SP600125, a specific inhibitor of JNK1/2, and pyrrolidine dithiocarbamate (PDTC), a specific inhibitor of NF-κB were purchased from Calbiochem (San Diego, CA). LY294002, a specific inhibitor of phosphatidylinositol 3-kinase (PI3K), was purchased from Sigma–Aldrich (St. Louis, MO).

2.2. Culture media

RPMI-1640 liquid medium was purchased from Sigma–Aldrich (St. Louis, MO) and supplemented with 100 IU/ml penicillin, 100 μg/ml streptomycin, and 50 μM 2-mercaptoethanol, and 5% fetal calf serum (FCS).

2.3. DC culture

Murine BMDCs were generated as previously described (Inaba et al., 1992). Wild type (WT) C57BL/6 (B6) mice were purchased from Japan SLC (Hamamatsu, Japan). $TLR2^{-/-}$ mice (B6 back ground) were generated previously (Takeuchi et al., 1999). Bone marrow cells were prepared from femur and tibial bone marrow of WT or $TLR2^{-/-}$ mice. After lysis of erythrocytes, MHC class II-, CD45R (B220)-, CD4-, and CD8-positive cells were removed by killing with mAbs (1E4, RA3-6B2, GK1.5, and 53-6.7) and rabbit complement. The cells were cultured in 5% FCS RPMI-1640 containing GM-CSF (20 ng/ml), at a density of 1×10^6 cells/ml/well (24-well plate). On day 2, the medium was gently exchanged to fresh medium. On day 4, non-adherent granulocytes were removed without dislodging clusters of developing DCs, and fresh medium was added. On day 6, free-floating and loosely adherent cells were collected and were used as BMDCs (>90% $CD11c^+$).

2.4. Measurement of IL-10, IL-12 p40, and TNF-α

DCs (2×10^5/ml) were treated with P3C and/or sLPS or upLPS for 24 h in 5% FCS RPMI-1640. sLPS and upLPS were used at 10, 30, 100, 300, or 1000 ng/ml. P3C was used at 100 ng/ml, based on our preliminary dose–response study. In some experiments, cells (2×10^5/ml) were pretreated with U0126, SB203580, LY294002, SP600125, PDTC, or vehicle alone (0.1% DMSO) for 1 h and then stimulated with upLPS (1 μg/ml) and/or P3C (100 ng/ml) for 24 h in the presence of each inhibitor. U0126, SB203580, SP600125, LY294002, and PDTC were used at 10, 30, 10, 10, and 20 μM, respectively, based on our preliminary dose–response study. The culture supernatants were subjected to quantification of the protein level of IL-10, IL-12 p40, and TNF-α by ELISA using OptEIA ELISA Set (BD Pharmingen, San Jose, CA).

2.5. Flow cytometry

Cell staining with FITC-, PE-, or biotin-conjugated mAb, and streptavidin-PerCP and flow cytometric analysis were performed on EPICS XL (Beckman Coulter Inc., Miami, FL) as previously described (Yanagawa et al., 2002).

2.6. Immunoblotting

DCs (7.5×10^5/ml) were treated with upLPS (1 μg/ml) and/or P3C (100 ng/ml) for the indicated time period. Reactions were halted by rapidly cooling on ice, and these cells were washed by ice-cold phosphate-buffered saline (PBS). The whole cell lysates were prepared using cell lysis buffer (Cell signaling Technology, Beverly, MA). The cell lysates were separated by SDS-PAGE, and then blotted onto a PVDF membrane (Millipore, Bedford, MA). The membrane were proved with primary Ab, and developed with HRP-conjugated secondary Ab by enhanced chemiluminescence.

3. Results

3.1. DC production of IL-10 and IL-12 upon sLPS or upLPS stimulation

LPS induces DC production of various cytokines including IL-10 and IL-12. In the present study, we used two types of LPS, normally prepared LPS (standard LPS, sLPS) and highly purified LPS (ultra-pure LPS, upLPS) to stimulate DCs. We first compared effects of sLPS and upLPS on IL-10 and IL-12 production by murine BMDCs that were positive for CD11b and negative for CD8 and B220 (data not shown), a pattern typical of conventional DCs.

BMDCs were treated with sLPS or upLPS (10–1000 ng/ml) for 24 h and levels of IL-10 and IL-12 in the culture supernatant were determined by ELISA. Both sLPS and upLPS similarly induced vig-

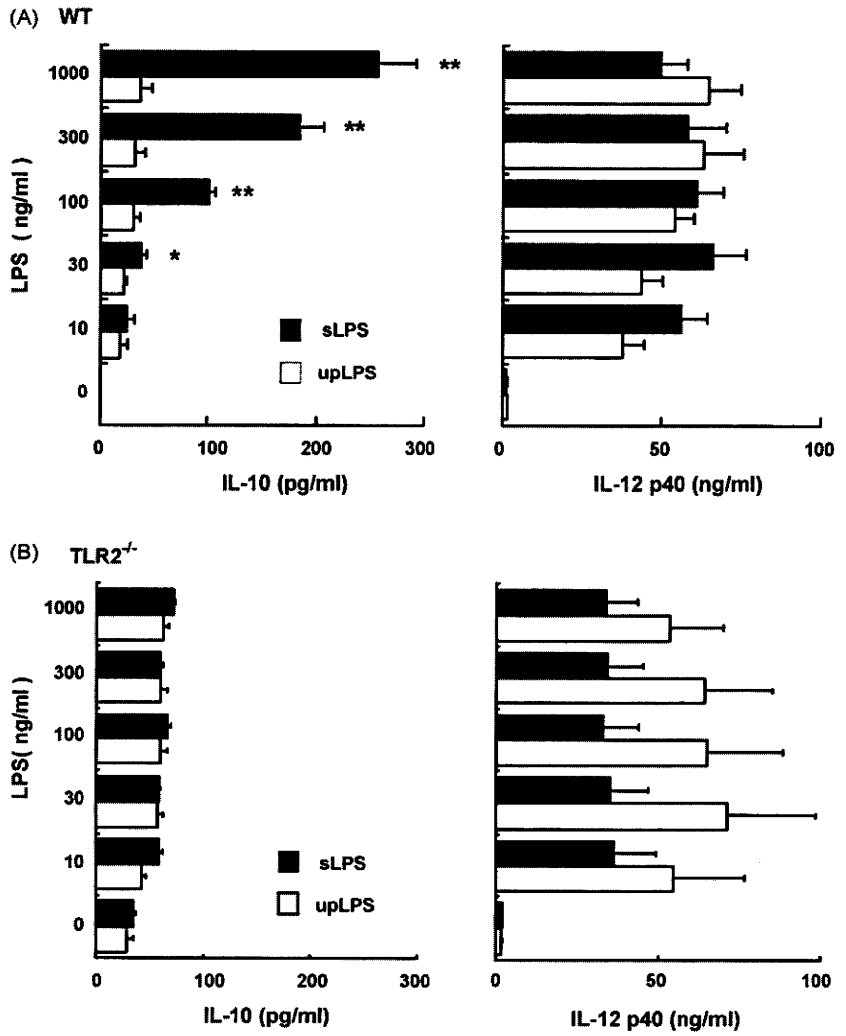

Fig. 1. IL-10 and IL-12 production by DCs upon sLPS or upLPS stimulation. BMDCs from WT (A) or TLR2$^{-/-}$ (B) mice were treated with sLPS or upLPS (10–1000 ng/ml) for 24 h. The amount of IL-10 and IL-12 in the culture supernatants was measured by ELISA. Each column represents the mean ± S.E. of three (B) or four (A) independent experiments. Statistical significance was calculated by paired *t*-test ($^{*}p < 0.05$; $^{**}p < 0.01$ vs. upLPS group).

orous production of IL-12 p40 by DCs (Fig. 1A right). sLPS also induced substantial levels of IL-10 production by DCs in a dose dependent manner (Fig. 1A left). In contrast, upLPS induced a negligible amount of IL-10 production by DCs compared to sLPS. We considered that contaminated bacterial components other than LPS might have contributed to the sLPS-induced IL-10 production by DCs.

The sLPS are generally contaminated with other bacterial components such as lipoproteins that activate TLR2-mediated signaling (Hirschfeld et al., 2000; Tapping et al., 2000; Hellman et al., 2003), whereas upLPS activates only TLR4-mediated signaling (David et al., 2005). To clarify the role of TLR2-mediated signaling in cytokine production by DCs upon sLPS stimulation, DCs prepared from TLR2 deficient (TLR2$^{-/-}$) mice were treated with sLPS or upLPS and then the levels of IL-10 and IL-12 production was determined (Fig. 1B). Either sLPS or upLPS only slightly increased IL-10 production by TLR2$^{-/-}$ DCs (Fig. 1B left). In contrast, both sLPS and upLPS induced vigorous production of IL-12 p40 by TLR2$^{-/-}$ DCs (Fig. 1B right). There were no significant differences in the production levels of IL-10 and IL-12 by TLR2$^{-/-}$ DCs between upLPS and sLPS groups. Thus, TLR2-mediated signaling appeared to be crucial for DC production of IL-10 but not IL-12 upon sLPS stimulation.

3.2. Synergistic enhancement of IL-10 production by DCs upon simultaneous treatment with TLR4 and TLR2 ligands

As described above, TLR2 activation by the contaminated bacterial components such as lipoproteins appeared to be involved in the substantial IL-10 production by DCs upon sLPS stimulation. P3C is a synthetic lipopeptide and a representative TLR2 ligand. We next examined cytokine production by DCs upon simultaneous stimulation with upLPS and P3C.

BMDCs were treated with P3C and/or either type of LPS (upLPS or sLPS) for 24 h and then the levels of IL-10, IL-12, and TNF-α in the culture supernatant were determined by ELISA (Fig. 2A). P3C alone failed to induce IL-10 production by DCs. upLPS slightly increased IL-10 production by DCs. Notably, simultaneous treatment of DCs with upLPS and P3C resulted in a synergistically augmented production of IL-10 and the level was similar to that of sLPS-induced IL-10 production (Fig. 2A left). The level of the sLPS-induced IL-10 production was unaffected by additional treatment with P3C. When TLR2$^{-/-}$ DCs were analyzed, the synergistic effect of the simultaneous treatment with upLPS and P3C was not observed as was shown with sLPS in Fig. 1B.

In contrast, DCs showed substantial production of IL-12 p40 and TNF-α in response to P3C, upLPS, or sLPS (Fig. 2A middle and right).

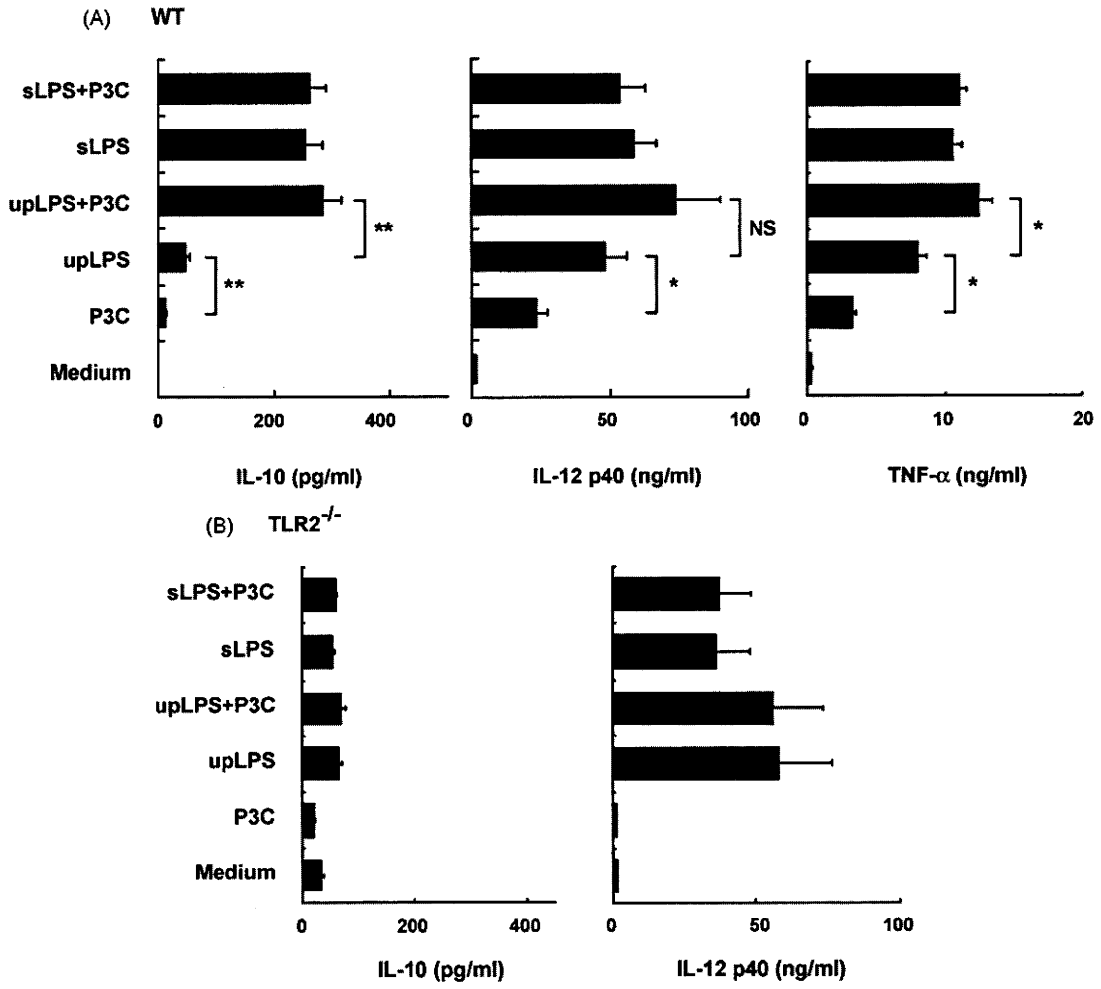

Fig. 2. Synergy in IL-10 production by DCs upon simultaneous treatment with upLPS and P3C. BMDCs from WT (A) or TLR2$^{-/-}$ (B) mice were treated with P3C (100 ng/ml) and/or upLPS (1 μg/ml) or sLPS (1 μg/ml) for 24 h. Each column represents the mean ± S.E. of three (B) or four (A) independent experiments. Statistical significance was calculated by paired *t*-test ($^{*}p < 0.05$; $^{**}p < 0.01$, NS: not significant).

The ability of upLPS or sLPS to induce IL-12 p40 and TNF-α production was considerably higher than that of P3C. No significant differences were detected in the level of IL-12 p40 production by DCs between single treatment with upLPS and simultaneous treatment with upLPS and P3C. The upLPS-induced TNF-α production was additively increased by an additional treatment with P3C. The sLPS-induced production of IL-12 p40 and TNF-α was unaffected by P3C addition. TLR2 deficiency completely abolished the IL-12 p40 production induced by P3C but not those by upLPS or sLPS (Fig. 2B right). We also analyzed IL-12 p70 production by DCs upon TLR stimulation. However, IL-12 p70 was not detected in any cultures examined (data not shown).

3.3. Cell surface expressions of maturation markers on TLR-stimulated DCs

We next analyzed cell surface expressions of maturation markers on DCs treated with sLPS, upLPS or P3C, and P3C in combination with upLPS or sLPS. BMDCs were treated with these TLR ligands for 24 h and the cell surface expressions of CD40, CD86, and I-A^{b} were determined by flow cytometry (Fig. 3). CD40 expression on DCs was significantly up-regulated after treatment with P3C, upLPS, or sLPS alone compared with those of medium control. The CD86 expression was also increased by treatment with either TLR ligand. The levels of CD40, CD86, and I-A^{b} expressions on DCs treated with either upLPS or sLPS were not significantly affected by the additional treatment with P3C.

3.4. MAPK activation in DCs upon TLR stimulation

TLR ligands activate MAPKs including ERK1/2, p38 MAPK, and JNK1/2 (O'Neill, 2006; O'Neill and Bowie, 2007). These MAPKs play crucial roles in regulating cytokine production by TLR-stimulated DCs (Nakahara et al., 2006). To clarify the mechanism underlying the synergistic enhancement of IL-10 production by DCs simultaneously stimulated with TLR4 and TLR2 ligands (TLR4,2-stimulated DCs), we quantitated and compared the MAPK activities between TLR4-, TLR2-, and TLR4,2-stimulated DCs.

BMDCs were treated with upLPS and/or P3C for indicated time periods, and intracellular proteins levels of phospho-ERK1/2, phospho-p38 MAPK, and phospho-JNK1/2 were determined using immunoblotting (Fig. 4). Marked phosphorylation of ERK1/2, p38 MAPK, and JNK1/2 was observed at 15 min after P3C stimulation and these levels of the phosphorylated MAPKs were gradually decreased at 30 and 60 min. In contrast, modest phosphorylation of ERK1/2, p38 MAPK, and JNK1/2 was shown in DCs at 15 min after upLPS stimulation. The levels of these phosphorylated MAPKs were markedly increased at 30 min, and then slightly decreased at 60 min. Accordingly, it was clearly shown in Fig. 4B that the levels of phospho-MAPKs induced by P3C stimulation were markedly

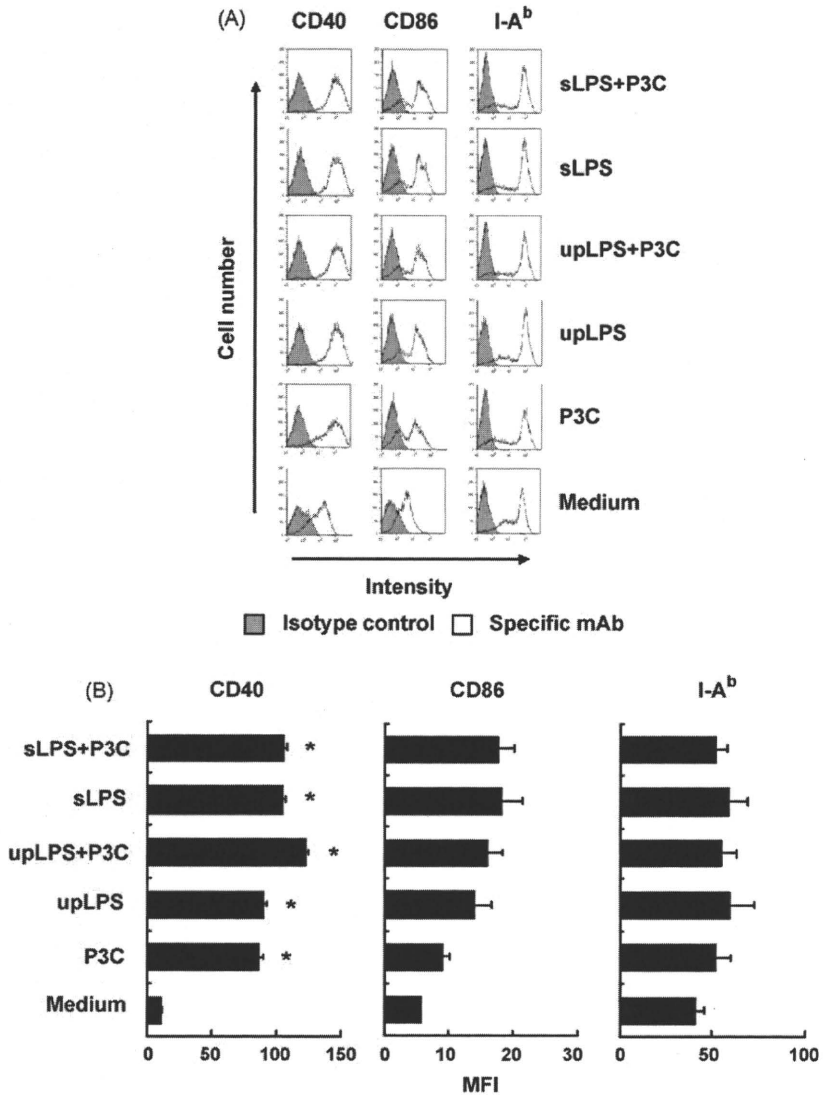

Fig. 3. Expression of surface molecules on TLR-stimulated DCs. BMDCs were treated with P3C (100 ng/ml) and/or upLPS (1 μg/ml) or sLPS (1 μg/ml) for 24 h. Expressions of CD40, CD86, and I-A^b were analyzed by flow cytometry. (A) Representative histogram of the each molecule on DCs. (B) Each column represents the mean ± S.E. of four independent experiments. MFI, mean fluorescence intensity. Statistical significance was calculated by paired *t*-test (*$p < 0.05$ vs. medium control).

higher than those by upLPS at 15 min. On the contrary, the levels of phospho-ERK1/2 or p38 MAPK in DCs stimulated with upLPS was higher than those stimulated with P3C at 30 and 60 min. Thus, the kinetics of the MAPKs activation appeared to be different between upLPS- and P3C-treated DCs.

The levels of phospho-MAPKs in DCs treated with both upLPS and P3C were considerably higher than those with upLPS alone at 15 min. On the other hand, the levels of MAPKs in DCs treated with the both ligands were at almost the same level as those of DCs stimulated with upLPS alone at 30 and 60 min. Thus, the simultaneous treatment of DCs with upLPS and P3C resulted in vigorous MAPK activation at the entire early phase (15–60 min) compared to that received single treatment with upLPS.

3.5. The role of MAPKs in cytokine production by DCs upon TLR stimulation

As compared to single treatment with upLPS or P3C, simultaneous treatment with these ligands resulted in the enhanced activation of MAPKs in DCs especially at 15 min after the stimulation (Fig. 4). To elucidate roles of MAPK pathways in the enhanced production of IL-10 by TLR4,2-stimulated DCs, blocking study was performed using U0126, a specific inhibitor of MEK1/2 that is required for ERK1/2 activation, SB203580, a specific inhibitor of p38 MAPK, and SP600125, a specific inhibitor of JNK1/2.

BMDCs were pretreated with U0126, SB203530, SP600125, or vehicle alone (0.1% DMSO) for 1 h and then stimulated with upLPS and/or P3C for 24 h in the presence of each inhibitor. Then the amounts of IL-10 and IL-12 p40 were quantitated by ELISA (Fig. 5). As was already demonstrated in Fig. 2, P3C failed to induce IL-10 production, and upLPS slightly induced IL-10 production by DCs. Simultaneous treatment of DCs with upLPS and P3C again resulted in the synergistic enhancement of IL-10 production by the DCs (Fig. 5). Either SB203530 or SP600125 almost completely inhibited the enhanced production of IL-10 by DCs treated with both upLPS and P3C. Although U0126 modestly decreased the IL-10 production by these DCs, the effect was statistically not significant. These findings demonstrate the activation of p38 MAPK and JNK1/2 are indispensable for IL-10 production. In contrast, these inhibitors showed no significant effects on IL-12 p40 production by DCs upon simultaneous treatment with upLPS and P3C. Thus, it appears that the activation of all MAPKs is not necessarily essential for IL-12 p40 production.